# Detrital zircon geochronology of pre-Tertiary strata in the Tibetan-Himalayan orogen

G. Gehrels,[1] P. Kapp,[1] P. DeCelles,[1] A. Pullen,[1] R. Blakey,[2] A. Weislogel,[3] L. Ding,[4] J. Guynn,[5] A. Martin,[6] N. McQuarrie,[7] and A. Yin[8]

[1]  Detrital zircon data have recently become available from many different portions of the Tibetan–Himalayan orogen. This study uses 13,441 new or existing U-Pb ages of zircon crystals from strata in the Lesser Himalayan, Greater Himalayan, and Tethyan sequences in the Himalaya, the Lhasa, Qiangtang, and Nan Shan–Qilian Shan–Altun Shan terranes in Tibet, and platformal strata of the Tarim craton to constrain changes in provenance through time. These constraints provide information about the paleogeographic and tectonic evolution of the Tibet–Himalaya region during Neoproterozoic to Mesozoic time. First-order conclusions are as follows: (1) Most ages from these crustal fragments are <1.4 Ga, which suggests formation in accretionary orogens involving little pre-mid-Proterozoic cratonal material; (2) all fragments south of the Jinsa suture evolved along the northern margin of India as part of a circum-Gondwana convergent margin system; (3) these Gondwana-margin assemblages were blanketed by glaciogenic sediment during Carboniferous–Permian time; (4) terranes north of the Jinsa suture formed along the southern margin of the Tarim–North China craton; (5) the northern (Tarim–North China) terranes and Gondwana-margin assemblages may have been juxtaposed during mid-Paleozoic time, followed by rifting that formed the Paleo-Tethys and Meso-Tethys ocean basins; (6) the abundance of Permian–Triassic arc-derived detritus in the Lhasa and Qiangtang terranes is interpreted to record their northward migration across the Paleo- and Meso-Tethys ocean basins; and (7) the arrival of India juxtaposed the Tethyan assemblage on its northern margin against the Lhasa terrane, and is the latest in a long history of collisional tectonism.

**Citation:** Gehrels, G., et al. (2011), Detrital zircon geochronology of pre-Tertiary strata in the Tibetan-Himalayan orogen, *Tectonics*, *30*, TC5016, doi:10.1029/2011TC002868.

## 1.  Introduction

[2]  It has been recognized since the earliest plate tectonic syntheses [e.g., *Chang and Zheng*, 1973; *Dewey and Burke*, 1973; *Şengör*, 1979; *Allégre et al.*, 1984; *Şengör et al.*, 1988; *Dewey et al.*, 1988] that the Tibetan Plateau consists of a collage of crustal fragments separated by oceanic sutures (Figure 1). Most fragments (or terranes) are dominated by marine strata and arc-type igneous rocks that formed along convergent plate boundaries during Paleozoic and early Mesozoic time [*Dewey et al.*, 1988; *Hsü et al.*, 1995; *Şengör and Natal'in*, 1996a, 1996b; *Yin and Harrison*, 2000]. The separating sutures commonly contain ophiolitic rocks and/or high-pressure metamorphic assemblages that record closure of intervening oceanic basins during Mesozoic and early Cenozoic time [*Yin and Harrison*, 2000; *Zhang and Tang*, 2009].

[3]  Current models for the tectonic development of Tibet and the Himalaya [e.g., *Metcalfe*, 1996; *Yin and Nie*, 1996; *Şengör and Natal'in*, 1996a; *Yin and Harrison*, 2000; *Blakey*, 2008] generally incorporate four phases of development, as follows:

[4]  1. Sequential rifting of crustal fragments from the northern (Tethyan) margin of Gondwana during Paleozoic and early Mesozoic time.

[5]  2. Displacement of the fragments northward across various smaller ocean basins in the Tethyan realm.

[1]Department of Geosciences, University of Arizona, Tucson, Arizona, USA.
[2]Department of Geology, Northern Arizona University, Flagstaff, Arizona, USA.
[3]Department of Geological Sciences, University of Alabama, Tuscaloosa, Alabama, USA.
[4]Institute of Tibetan Plateau Research, Chinese Academy of Sciences, Beijing, China.
[5]ExxonMobil Exploration Company, Houston, Texas, USA.
[6]Department of Geology, University of Maryland, College Park, Maryland, USA.
[7]Department of Geological Sciences, Princeton University, Princeton, New Jersey, USA.
[8]Department of Earth and Space Sciences, University of California, Los Angeles, California, USA.
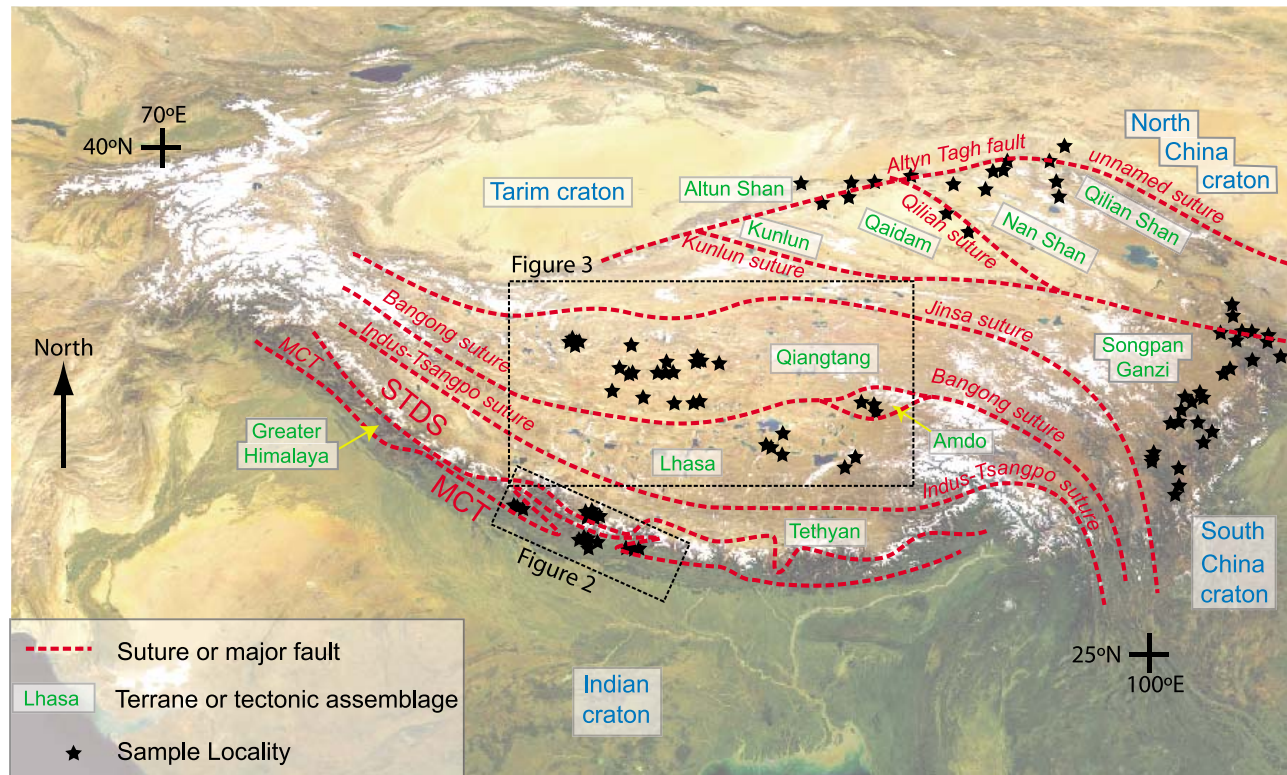
**Figure 1.** Satellite image of the Tibet–Himalayan orogen showing main cratons, terranes and tectonic assemblages, and first-order sutures and structures. Adapted from *Yin and Harrison* [2000] and *Hodges* [2000]. Detrital zircon sample localities are shown with stars. Base Image from Terra satellite (NASA).

[6] 3. Progressive accretion of each fragment against the North China and Tarim cratons (southern margin of Laurasia), through subduction and eventual closure of the intervening ocean basins.

[7] 4. Final closure of the Tethyan oceanic realm, and formation of the Tibetan–Himalayan orogen, with the arrival of India during latest Cretaceous–early Tertiary time.

[8] Although this simple model is supported by a wealth of geologic relations, paleomagnetic data, and biogeographic information, significant uncertainties remain on where each fragment originated along the Tethyan margin, where the boundary resides between Gondwanan and Laurasian fragments, and when each fragment was accreted along the northern margin of the Tethyan realm. This study uses detrital zircon U-Pb geochronologic data from the main terranes in Tibet and the Himalaya (Figure 1) to address these questions and thereby improve our understanding of the tectonic history of Paleozoic and Mesozoic rocks that make up much of the Tibetan–Himalayan orogen. Key strategies for using detrital zircon data for this purpose, as outlined by *Gehrels* [2000, 2011], *Fedo et al.* [2003], and *Andersen* [2005], are as follows:

[9] 1. The objective of analyzing detrital zircon grains is to produce an age distribution that accurately reflects the true distribution of ages in a sample. Biases introduced during data analysis and presentation are minimized.

[10] 2. An age distribution from a sample generally reflects the ages of zircons in the source rocks for the sediment. However, there are many geologic factors that bias this age distribution, including recycling of zircons from older sedimentary units exposed in the source region, incorporation of detrital zircons during transport, preferential elimination of older or high-U grains (due to loss of durability from enhanced Pb loss), variations in zircon fertility in different source rocks, and changes in proportions of ages as different sources are introduced or removed.

[11] 3. Because of these biases, comparisons of age distributions are most reliable if based primarily on the presence of specific ages or age groups. The absence of a particular age or age group may also be useful, although the absence may be due to sampling or analytical bias, especially if it is a minor component in the sample. Variations in proportions of ages are used with caution.

[12] 4. A detrital zircon age distribution from a sedimentary unit provides information about the sources from which the zircons were derived, and also provides a reference that can be used to determine whether the unit was a source for sediment in younger units. A group of samples can be combined to characterize a region or terrane for either purpose, but the reliability of this reference will depend on the number of samples analyzed, their age range and geographic distribution, and the heterogeneity of the detrital zircon age distributions.

[13] 5. The age of an individual zircon grain is used with caution, even if the analysis is precise and concordant, because of the possibility that the grain has been compromised by Pb loss or inheritance. Interpretations are accordingly most reliable if based on several overlapping analyses,
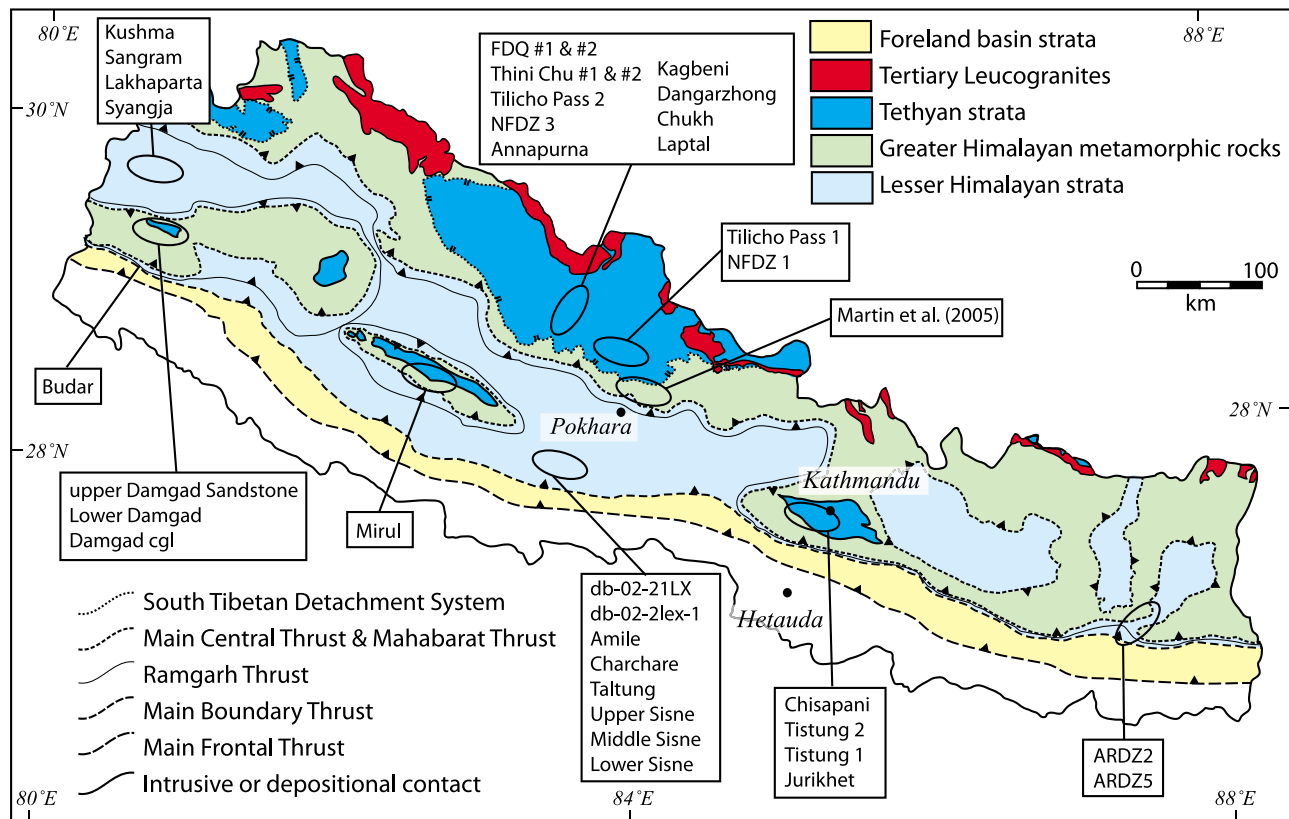
**Figure 2.** Geologic assemblages and major structures of Nepal, with approximate locations of detrital zircon samples. Note that some samples have been described by others, as noted. Geologic map adapted from *DeCelles et al.* [2004].

because Pb loss and inheritance will generally serve to disperse (rather than concentrate) ages.

## 2. Terranes and Sutures in the Tibetan–Himalayan Orogen

[14] The primary cratons, crustal fragments (terranes), and separating structures (commonly sutures but also large-scale strike-slip faults) recognized in Tibet and the Himalaya are shown on Figures 1–3 and are briefly described in the following sections. These descriptions are keyed to schematic stratigraphic columns, shown in Figure 4. For more information about the assemblages and sutures that make up the Tibetan–Himalayan orogen, refer to the excellent syntheses by *Şengör and Natal'in* [1996a], *Hodges* [2000], *Yin and Harrison* [2000], and *Yin* [2006]. From south to north, the main assemblages are as follows:

### 2.1. Indian Craton and Lesser Himalayan Strata

[15] The northern Indian craton consists of Archean and Early Proterozoic granitoids and gneisses, and of Lower and Middle Proterozoic sedimentary and metasedimentary assemblages [*Goodwin*, 1996; *Kohn et al.*, 2010]. These rocks are overlain by Neoproterozoic–Cambrian (and possibly Ordovician [*McQuarrie et al.*, 2008]), Carboniferous–Permian, and Mesozoic [*Gansser*, 1964; *Sakai*, 1991; *Brookfield*, 1993; *Upreti*, 1999; *Hodges*, 2000; *DeCelles et al.*, 2001; *Myrow et al.*, 2003, 2009, 2010; *Hughes et al.*, 2005; *Yin et al.*, 2010a, 2010b; *Martin et al.*, 2011] strata.

Paleo- and Mesoproterozoic sedimentary and metasedimentary units, referred to as the lower LHS, may have formed as a passive margin sequence, although *Kohn et al.* [2010] suggest that 2.1–1.8 Ga orthogneiss at the base of this sequence may have formed in a Paleoproterozoic arc along the northern (present coordinates) margin of India. Neoproterozoic and younger strata are referred to as the upper LHS, and include Carboniferous through Cretaceous strata that belong to the Gondwana sequence [*Gansser*, 1964; *Sakai*, 1991; *Upreti*, 1999]. These upper LHS strata clearly formed along a passive margin, with rifting during Late Proterozoic, Permian, and Cretaceous time [*Brookfield*, 1993; *Garzanti*, 1999; *Myrow et al.*, 2003, 2010]. The lack of mid-Paleozoic strata may be due to uplift and erosion or non-deposition resulting from an early Paleozoic orogenic event [*Brookfield*, 1993; *Gehrels et al.*, 2003; *Cawood et al.*, 2007; *Martin et al.*, 2007; *McQuarrie et al.*, 2008; *Yin et al.*, 2010b; *Johnson et al.*, 2001]. All of the Lesser Himalayan strata are found in frontal (southern) portions of the Himalaya (Figures 1 and 2).

### 2.2. Greater Himalayan Rocks

[16] The Greater Himalayan Sequence in Nepal consists of three different units: a lower assemblage (Formation I) of pelitic to psammitic biotite schist and paragneiss derived from sandstone, mudstone, and shale (locally with graded bedding); a middle sequence (Formation II, locally absent) of marble and calc-silicate gneiss; and an upper unit (Formation III) of mainly orthogneiss derived from
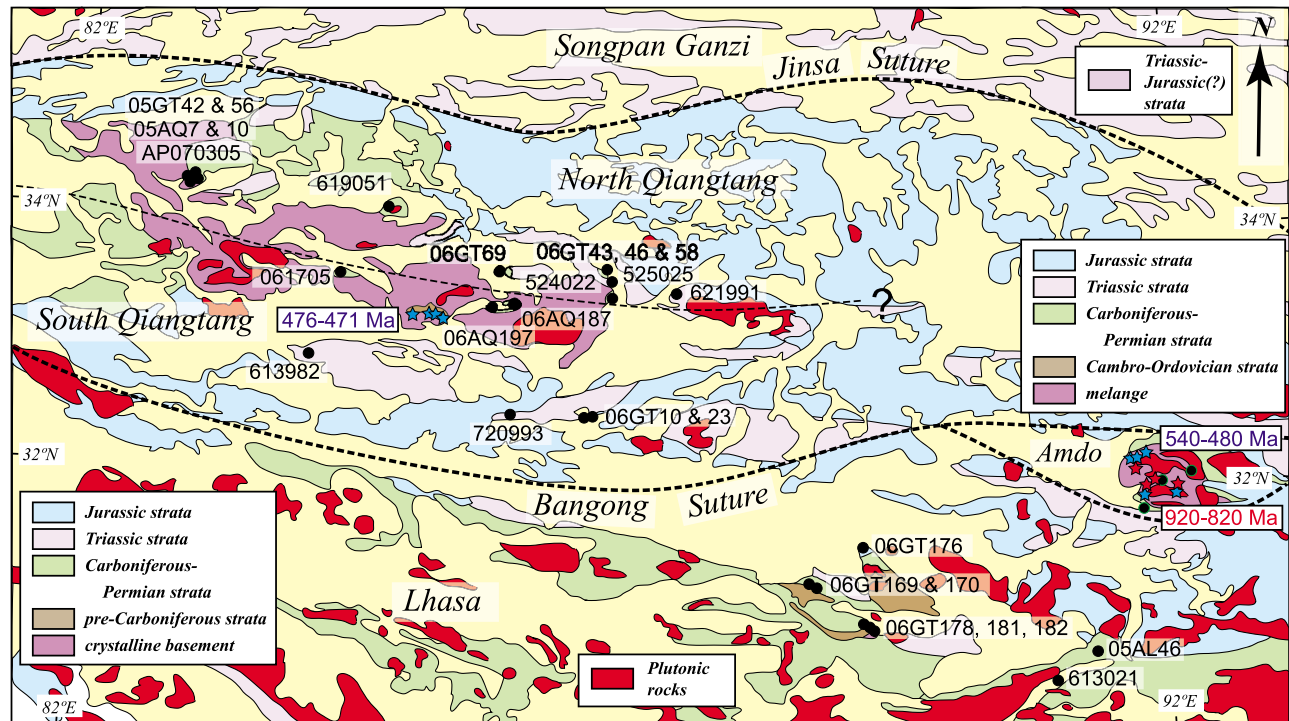
**Figure 3.** Geologic assemblages and major structures of central Tibet, with approximate locations of detrital zircon samples. Note that some samples have been reported by *Guynn et al.* [2006, 2011] and *Pullen et al.* [2010]. Also shown (in blue) are crystalline ages from igneous rocks in South Qiangtang [from *Pullen et al.*, 2010] and the Amdo basement [from *Guynn et al.*, 2006, 2011]. Geologic map adapted from *Pan et al.* [2004].

Ordovician granitic rocks [*Gansser*, 1964; *Bordet et al.*, 1971; *Colchen et al.*, 1986; *Gehrels et al.*, 2003]. In higher portions of the Himalaya, these rocks structurally overlie Lesser Himalayan strata along a system of Cenozoic thrust faults that are referred to as the Main Central Thrust (MCT; Figure 2). These rocks also are present to the south, in isolated klippen that crop out in frontal portions of the Himalaya, where they structurally overlie Lesser Himalayan strata along the Mahabharat thrust (Figure 2). Note that there are also regions in the northwestern Himalaya where Greater Himalayan rocks are not present, and Tethyan strata (described below) are thrust directly over Lesser Himalayan strata [*Webb et al.*, 2007].

[17] Previous models have suggested that Greater Himalayan protoliths accumulated during late Proterozoic and Cambrian time along the northern margin of Greater India [*Parrish and Hodges*, 1996; *DeCelles et al.*, 2000; *Myrow et al.*, 2003; *Gehrels et al.*, 2003; *Myrow et al.*, 2009]. Protoliths may have accumulated as the northern equivalent of Neoproterozoic strata of the Vindyan series on the Indian craton [*Parrish and Hodges*, 1996], as an offshelf sequence of uncertain paleoposition within the paleo-Tethys oceanic basin [*DeCelles et al.*, 2000], or as correlatives of Neoproterozoic–Cambrian strata of the Lesser Himalayan and Tethyan sequences [*Myrow et al.*, 2003, 2009, 2010; *Gehrels et al.*, 2003]. Tectonic juxtaposition of these rocks over Lesser Himalayan strata may have occurred initially during early Paleozoic time [e.g., *Gehrels et al.*, 2003; *Martin et al.*, 2007], with the main phase of overthrusting during

latest Cretaceous–early Tertiary India–Asia collision [*Searle et al.*, 1987; *Hodges*, 2000; *Yin*, 2006].

### 2.3. Tethyan Strata

[18] The Tethyan sequence consists of dominantly marine clastic strata and carbonate rocks that overlie Greater Himalayan metamorphic rocks both in the lower (frontal) and higher portions of the Himalaya. In the higher Himalaya, Tethyan strata are separated from the Greater Himalayan Sequence by normal faults of the South Tibetan Detachment Fault System (STDS of Figures 1 and 2 [*Hodges*, 2000]). In the frontal Himalaya in Nepal the basal contact is instead an unconformity, with Ordovician strata overlying Greater Himalayan metasedimentary equivalents [*Gehrels et al.*, 2006a, 2006b].

[19] Tethyan strata in Nepal and northwestern India range in age from Neoproterozoic (?)–Cambrian through Paleogene [*Heim and Gansser*, 1939; *Gansser*, 1964; *Brookfield*, 1993; *Garzanti*, 1999; *Upreti*, 1999; *Myrow et al.*, 2006a, 2006b, 2010], with the younger limit defined by the influx of Eocene foreland basin strata resulting from Himalayan thrusting. Tethyan strata are interpreted to have formed along the southern margin of Tethyan ocean basins in response to Late Proterozoic, Carboniferous–Permian, and Cretaceous phases of rifting [*Gaetani and Garzanti*, 1991; *Brookfield*, 1993; *Garzanti*, 1999; *Hu et al.*, 2009].

### 2.4. Indus–Tsangpo Suture Zone

[20] This suture zone, as outlined by *Burg and Chen* [1984] and *Hodges* [2000], consists of ophiolites, ophio-
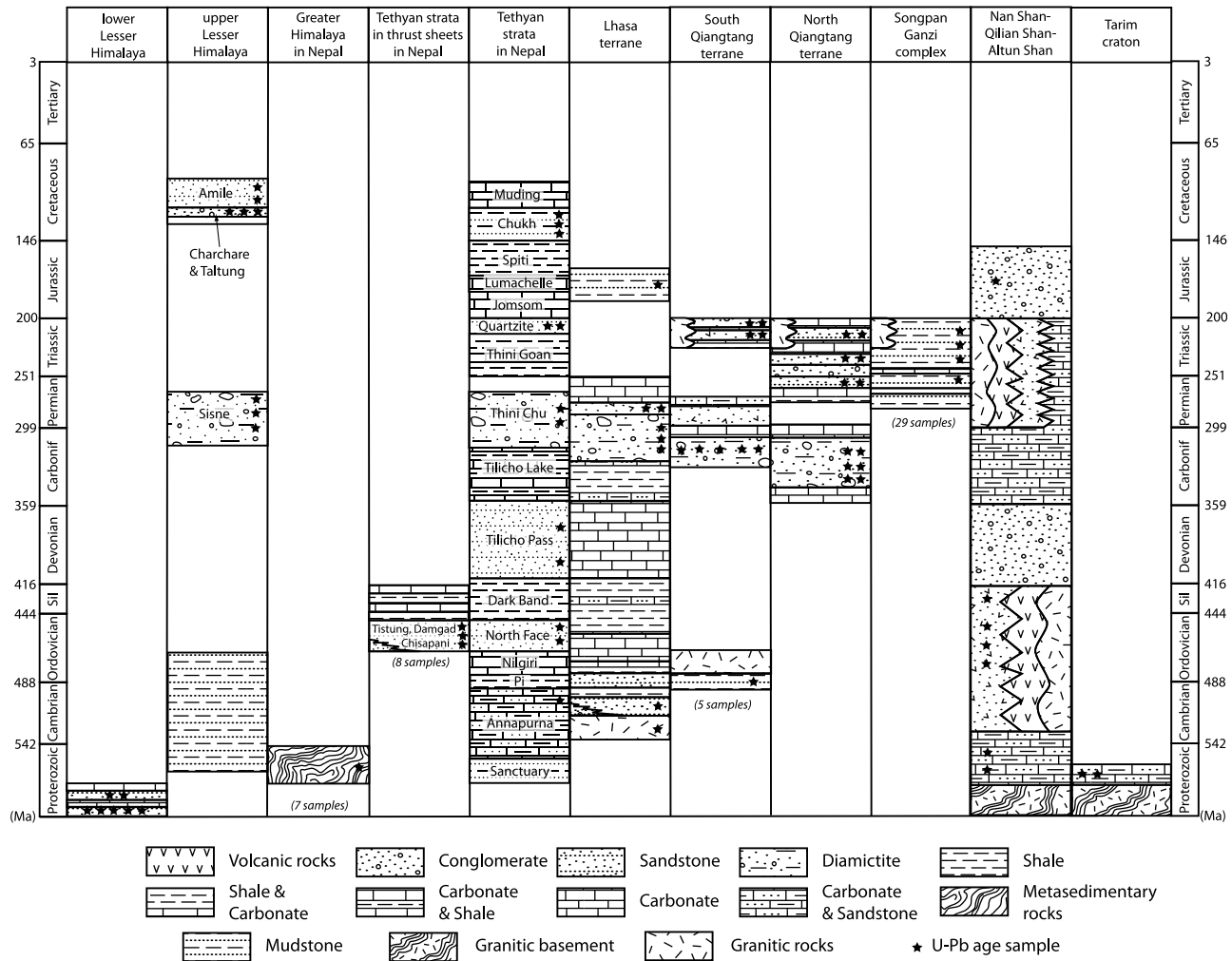
**Figure 4.** Simplified stratigraphy of the various terranes and assemblages analyzed, with emphasis on units analyzed as part of this study. Approximate position of detrital zircon samples reported herein shown with stars. Sources of information as follows: Lesser Himalayan strata in Nepal, northern India, and Bhutan [from *Sakai*, 1991; *Upreti*, 1999; *DeCelles et al.*, 2001, 2004; *Myrow et al.*, 2003; *Martin et al.*, 2011]; Greater Himalaya in Nepal [*Parrish and Hodges*, 1996; *Martin et al.*, 2005; *McQuarrie et al.*, 2008; *Gehrels et al.*, 2006a, 2006b]; Tethyan thrust sheets in Nepal [*Stöcklin and Bhattarai*, 1977; *Stöcklin*, 1980; *Upreti*, 1999; *Gehrels et al.*, 2006b, 2006c]; Tethyan strata in the higher Himalaya in Nepal [*Bordet et al.*, 1971; *Colchen et al.*, 1986; *Fuchs et al.*, 1988; *Garzanti*, 1999; *Upreti*, 1999]; Qiangtang terrane [*Li and Zheng*, 1993; *Li et al.*, 1995, 2006; *Kapp et al.*, 2000, 2003; *Pullen et al.*, 2010]; Nan Shan–Qilian Shan–Altun Shan [*Pan et al.*, 2004; *Gehrels and Yin*, 2003b].

litic melange, and deep-marine sedimentary rocks, locally with associated high-pressure metamorphic assemblages. Thick sequences of Cretaceous marine clastic strata immediately north of the suture (e.g., Xigaze Group) are generally interpreted to have formed in a fore-arc basin along the south-facing Gangdese arc, which is built on the southern margin of the Lhasa terrane [*Dürr*, 1996]. Most data sets are consistent with closure of the suture zone, and resultant accretion of India, to southern Asia during latest Cretaceous to Eocene time [*Hodges*, 2000; *Yin and Harrison*, 2000; *DeCelles et al.*, 2004; *Ding et al.*, 2003; *Leech et al.*, 2005; *Najman et al.*, 2005; *Garzanti*, 2008; *Ali and Aitchison*, 2008]. We have not analyzed pre-Cretaceous samples from this assemblage.

### 2.5. Lhasa Terrane

[21] This terrane consists mainly of Paleozoic and Mesozoic marine strata and arc-type volcanic rocks that are intruded by Jurassic through early Tertiary granitoids of the Gangdese batholith [*Yin and Harrison*, 2000]. These rocks were originally interpreted to rest unconformably on Neoproterozoic–Cambrian crystalline rocks of the Amdo terrane, although whether Amdo crystalline rocks represent basement of Lhasa or Qiangtang affinity, or both, is ambiguous [*Harris et al.*, 1988a, 1988b; *Guynn et al.*, 2006, 2011] due to their location within the Bangong suture zone (Figures 1 and 3). The northern margin of the Lhasa terrane is defined by the Bangong suture zone, which is interpreted to have closed diachronously during Late Jurassic–Early

Cretaceous time [*Dewey et al.*, 1988; *Yin and Harrison*, 2000]. Studies in the interior of the Lhasa terrane reveal a belt of eclogites that may mark a Permian rift overprinted by a suture [*Metcalfe*, 1996; *Pan et al.*, 2006; *Yang et al.*, 2009; *Zhu et al.*, 2009, 2010]. It is accordingly possible that Lhasa consists of two separate crustal fragments, or a single fragment that was separated for a short time by a small ocean basin or underplated by eclogitic material from the Indus–Tsangpo or Bangong sutures.

## 2.6. Bangong Suture

[22] This suture zone formed in response to closure of the Meso-Tethys ocean basin, which separated the Lhasa and Qiangtang terranes [*Dewey et al.*, 1988; *Yin and Nie*, 1996; *Kapp et al.*, 2003; *Baxter et al.*, 2009]. Primary components include Jurassic marine shale and conglomeratic strata, mélange, volcanic rocks, rare ophiolitic fragments, and high-pressure assemblages. Subduction was apparently northward beneath the Lhasa terrane, and/or intervening island arc systems, with final closure during Middle Jurassic to Early Cretaceous time [*Yin and Harrison*, 2000; *Kapp et al.*, 2007; *Baxter et al.*, 2009]. Pre-Cretaceous strata have not been analyzed from this assemblage.

## 2.7. Amdo Basement

[23] The Amdo terrane is the largest (~50 km × 70 km), and one of the few, exposures of crystalline basement in central and southern Tibet (Figure 3). It is located along the northern edge of the Bangong suture zone and is composed predominantly of high-grade orthogneisses intruded by Jurassic granitoids [*Xu et al.*, 1985; *Harris et al.*, 1988b; *Guynn et al.*, 2006, 2011]. It has generally been considered to represent Lhasa basement [*Coward et al.*, 1988], though the presence of Jurassic magmatism and metamorphism suggests ties with the Qiangtang terrane (described below) [*Guynn et al.*, 2006]. However, as the Lhasa and Qiangtang terranes are thought to have been together prior to Permo–Triassic rifting [*Leeder et al.*, 1988; *Dewey et al.*, 1988; *Yin and Harrison*, 2000], the Amdo terrane may represent Lhasa and Qiangtang crystalline crust. Two phases of magmatism are recorded in the orthogneisses, 820–920 Ma and 480–540 Ma (Figure 3) [*Guynn et al.*, 2011]. The younger magmatism indicates that southern Tibet was involved in the Cambro–Ordovician tectonism along Gondwana's northern margin [*Gehrels et al.*, 2003; *Cawood et al.*, 2007]. The older ages document the oldest known crust in southern Tibet, though isotopic data from the gneiss suggest that melting of even older Mesoproterozoic basement may have contributed to the orthogneiss protoliths [*Harris et al.*, 1988a].

## 2.8. Qiangtang Terrane

[24] This terrane consists of variably deformed and metamorphosed metasedimentary basement of probable latest Proterozoic–early Paleozoic age that is structurally overlain by a thick and widespread sequence of Carboniferous through Triassic marine strata and mafic volcanic rocks [*Yin and Harrison*, 2000; *Kapp et al.*, 2000, 2003; *Pan et al.*, 2004; *Pullen et al.*, 2008]. Some of the metamorphic rocks contain high-pressure assemblages [*Hennig*, 1915; *Li et al.*, 1995; *Kapp et al.*, 2000; *Zhang et al.*, 2006a, 2006b; *Pullen et al.*, 2008; *Zhang and Tang*, 2009], and

have been interpreted by some workers to form a suture zone separating distinct northern and southern blocks [e.g., *Li*, 1987; *Kidd et al.*, 1988; *Metcalfe*, 1988; *Şengör et al.*, 1988; *Li et al.*, 1995, 2006; *Metcalfe*, 1996; *Zhang*, 2001]. However, *Kapp et al.* [2000, 2003] and *Pullen et al.* [2008] suggest that the metamorphic rocks were underthrust from the Jinsa suture to north. The southern Qiangtang terrane also contains a local exposure of Cambrian (?) metasedimentary rocks intruded by Ordovician granitic bodies which are structurally overlain by the more typical Carboniferous through Jurassic strata [*Pullen et al.*, 2010].

## 2.9. Songpan–Ganzi Complex

[25] This assemblage consists primarily of Upper Triassic marine strata and, in southern portions of the terrane, arc-type volcanic rocks [*Yin and Harrison*, 2000; *Roger et al.*, 2004; *Weislogel et al.*, 2006; *Weislogel*, 2008]. Provenance studies and mass balance calculations suggest that most of the strata were shed from the Qinling–Dabie orogen to the east (which closed during Triassic collision between the North China and South China cratons), as well as from the Kunlun arc (to the north), the North China craton, and the South China craton [*Nie et al.*, 1994; *Zhou and Graham*, 1996; *Bruguier et al.*, 1997; *Weislogel et al.*, 2006; *Enkelmann et al.*, 2007; *Wang et al.*, 2009].

## 2.10. Jinsa Suture Zone

[26] The Late Triassic–Early Jurassic Jinsa suture is well-defined in eastern Tibet, where ophiolitic melange is found within and on either side of a narrow belt of Triassic arc-related rocks (e.g., Yidun island arc belt [*Dewey et al.*, 1988; *Reid et al.*, 2005; *Pullen et al.*, 2008]). To the west, its trace is defined by a few exposures of widely scattered ophiolitic fragments as it is mostly covered by early Tertiary strata associated with the development of the Fenghuo Shan thrust belt [*Pan et al.*, 2004]. It is uncertain whether the Jinsa suture accommodated subduction southward beneath Qiangtang [*Pearce and Mei*, 1988; *Yin and Harrison*, 2000; *Roger et al.*, 2004], northward beneath oceanic lithosphere [*Coward et al.*, 1988; *Li et al.*, 1995], or both [*Leeder et al.*, 1988]. We have not analyzed samples from this assemblage.

## 2.11. Kunlun–Qaidam Terrane

[27] This terrane consists mainly of Paleozoic and lower Mesozoic rocks that record arc-type magmatism during early Paleozoic and Permo–Triassic time [*Yin and Harrison*, 2000]. These rocks are referred to as the Kunlun batholith, which apparently formed in a long-lived south-facing subduction system [*Harris et al.*, 1988a; *Xiao et al.*, 2002]. Proterozoic basement is included to the west. This terrane is interpreted to make up the southern continuation of the Nan Shan–Qilian Shan–Altun Shan terrane (described below), at least following the closure of Ordovician–Silurian suture zones along their boundary [e.g., *Mattinson et al.*, 2006; *Yin et al.*, 2007]. Unfortunately, no detrital zircon data are available from pre-Cretaceous rocks of the Kunlun–Qaidam region.

## 2.12. Nan Shan–Qilian Shan–Altun Shan Terrane(s)

[28] The northeastern portion of the Tibetan Plateau is underlain by various Proterozoic basement complexes, lower Paleozoic rocks that formed in an arc-type setting,

and Carboniferous through Jurassic platformal strata [*Yin and Harrison*, 2000]. *Gehrels and Yin* [2003a, 2003b] conducted U-Pb analyses of plutons and strata from various portions of the terrane and, following the suggestion of *Sobel and Arnaud* [1999], concluded that it consists of a coherent north-facing early Paleozoic arc system that was accreted to the southern margin of the North China–Tarim craton during Ordovician–Silurian time. Subduction along the southern margin of this crustal fragment, as recorded in the Kunlun Shan, apparently continued until Triassic time [*Yin and Harrison*, 2000; *Pullen et al.*, 2008].

## 2.13.  North China/Tarim Craton

[29] The Tibetan Plateau is bounded to the north by the Tarim craton in the west and the North China craton in the east [*Metcalfe*, 1996; *Yin and Nie*, 1996]. These cratonal regions consist of Archean and Paleoproterozoic crystalline basement overlain by a platformal sequence of Proterozoic and Paleozoic age [*Pan et al.*, 2004; *Darby and Gehrels*, 2006].

## 3.  Analytical Methods

[30] Zircon crystals were extracted from 3 to 10 kg samples by traditional methods of crushing and grinding, followed by separation with a Wilfley table, heavy liquids, and a Frantz magnetic separator. Samples were processed such that as many zircons as possible were retained in the final heavy mineral fraction. A split of ~1000 zircon crystals, separated to include all grain sizes, was incorporated into a 1″ epoxy mount together with fragments of our Sri Lanka standard zircon. The mounts were sanded down to a depth of ~20 microns, polished, imaged (optically), and cleaned prior to isotopic analysis.

[31] U-Pb geochronology of zircons was conducted by laser ablation multicollector inductively coupled plasma mass spectrometry (LA–MC–ICPMS) at the Arizona LaserChron Center [*Gehrels et al.*, 2006c, 2008]. The analyses involve ablation of zircon with a New Wave DUV193 Excimer laser (operating at a wavelength of 193 nm) using a spot diameter of 35 microns. The ablated material is carried in helium into the plasma source of a GVI Isoprobe, which is equipped with a flight tube of sufficient width that U, Th, and Pb isotopes are measured simultaneously. All measurements are made in static mode, using Faraday detectors with $10^{11}$ ohm resistors for $^{238}U$, $^{232}Th$, $^{208}Pb$, and $^{206}Pb$, a Faraday detector with a $10^{12}$ ohm resistor for $^{2007}Pb$, and an ion-counting channel for $^{204}Pb$. Ion yields are ~1.0 mv per ppm. Each analysis consists of one 12-s integration on peaks with the laser off (for backgrounds), 12 one-second integrations with the laser firing, and a 30 s delay to purge the previous sample and prepare for the next analysis. The ablation pit is ~12 microns in depth.

[32] For each analysis, the errors in determining $^{206}Pb/^{238}U$ and $^{206}Pb/^{204}Pb$ result in a measurement error of ~1–2% (at 2-sigma) in the $^{206}Pb/^{238}U$ age. The errors in measurement of $^{206}Pb/^{207}Pb$ and $^{206}Pb/^{204}Pb$ also result in ~1–2% uncertainty (at 2-sigma) in age for grains that are >1.0 Ga, but are substantially larger for younger grains due to low intensity of the $^{207}Pb$ signal. The crossover in precision of $^{206}Pb/^{238}U$ and $^{206}Pb/^{207}Pb$ ages occurs at ~1.0 Ga,

but this cutoff value is adjusted for each sample to avoid dividing clusters of ages near 1.0 Ga.

[33] Common Pb correction is accomplished by using the measured $^{204}Pb$ and assuming an initial Pb composition from *Stacey and Kramers* [1975] (with 2-sigma uncertainties of 1.5 for $^{206}Pb/^{204}Pb$ and 0.3 for $^{207}Pb/^{204}Pb$). Our measurement of $^{204}Pb$ is unaffected by the presence of $^{204}Hg$ because backgrounds are measured on peaks (thereby subtracting any background $^{204}Hg$ and $^{204}Pb$), and because very little Hg is present in the argon plasma gas (background $^{204}Hg$ = ~300 counts per second).

[34] Inter-element fractionation of Pb/U is generally ~20%, whereas apparent fractionation of Pb isotopes is <1%. In-run analysis of fragments of a large zircon crystal (generally every fifth measurement) with known age of 563.5 ± 3.2 Ma (2-sigma) is used to correct for this fractionation. The uncertainty resulting from the calibration correction is generally 1–2% (2-sigma) for both $^{206}Pb/^{207}Pb$ and $^{206}Pb/^{238}U$ ages. Uncertainties from this calibration correction are combined (quadratically) with the uncertainty of the age of the standard, the U decay constants, and the assumed common Pb composition to yield an external uncertainty for each sample. This external uncertainty is reported for each sample in the auxiliary material tables and provides a minimum uncertainty for each analysis and set of analyses (e.g., a peak in age probability comprising several analyses).[1] Concentrations of U and Th are calibrated relative to our Sri Lanka zircon, which has ~518 ppm U and ~68 ppm Th.

[35] The analytical data are reported in Tables S1–S8. Reported uncertainties are at the 1-sigma level, and include only internal (measurement) errors for individual analyses. As noted above, external uncertainties for each sample are also reported, and provide a minimum uncertainty on sets of ages (e.g., a peak on an age-distribution diagram). Analyses that are >30% discordant (by comparison of $^{206}Pb/^{238}U$ and $^{206}Pb/^{207}Pb$ ages) or >5% reverse discordant are not considered further. Acceptance of analyses with up to 30% discordance allows us to include most of the age information from each sample, and therefore yields a more complete and accurate description of provenance components. For example, using a more stringent discordance filter (e.g., 10%) would preferentially remove older and/or higher U zircons from an age distribution given that Pb loss generally becomes more severe with increasing age.

[36] To ensure that grains with a complex history (e.g., inheritance, Pb loss, or overgrowths) do not compromise data quality, the time-resolved pattern of $^{206}Pb/^{238}U$ is monitored closely during acquisition, and any analyses that show unusual patterns (e.g., different fractionation from standards or jumps in value) are rejected [e.g., *Gehrels*, 2011, p. 186]. In addition, provenance interpretations are based primarily on age clusters that include at least three analyses, as inheritance, Pb loss, and/or multidomain analyses will almost always increase scatter [*Gehrels*, 2011].

[37] The resulting interpreted ages are shown on Pb*/U concordia diagrams (Figures S1–S7; from *Ludwig* [2008]) and age-distribution (relative age-probability) diagrams (Figures 5–11). These diagrams show each age and its
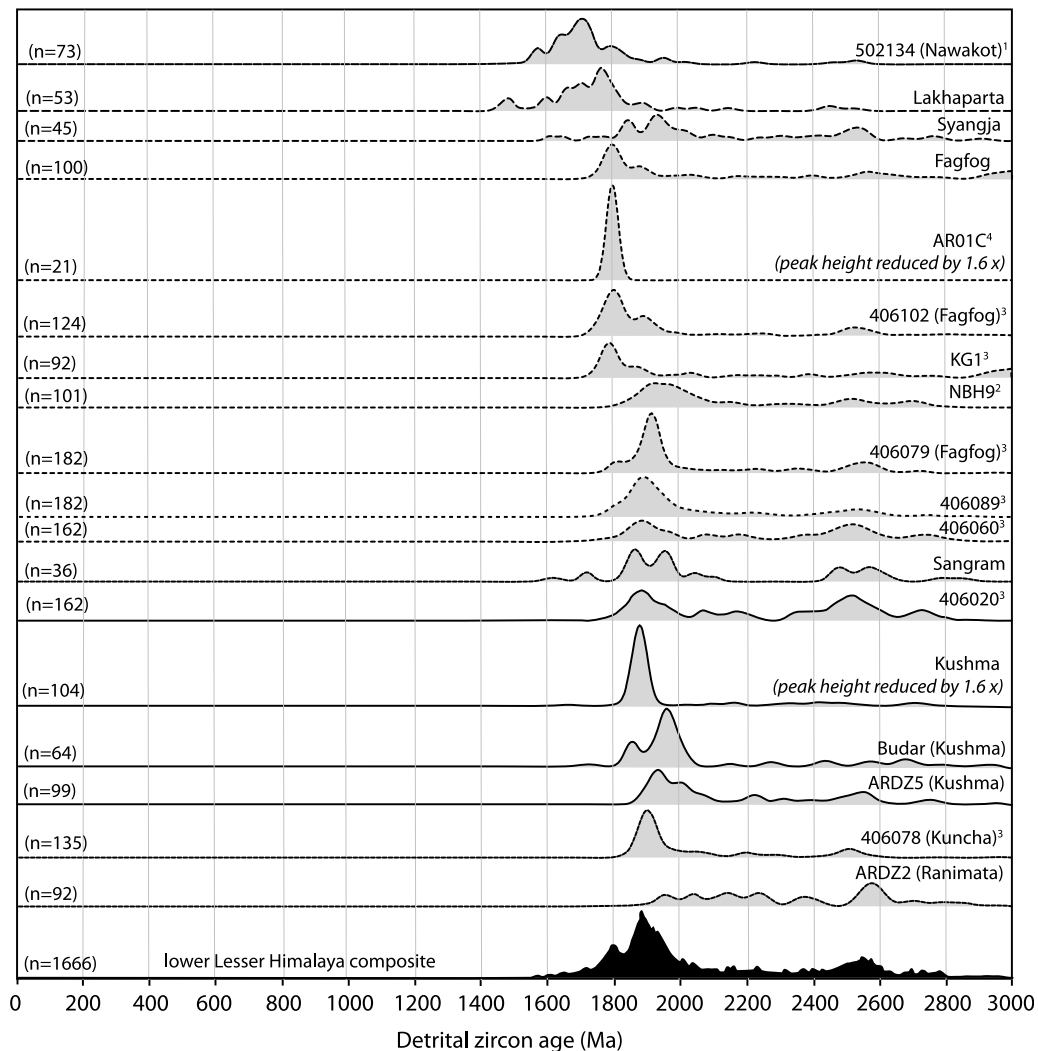
---

**Figure 5.** Normalized probability plots for lower Lesser Himalayan strata (Paleo- and Mesoproterozoic in age). Several samples were previously analyzed with ID–TIMS by *DeCelles et al.* [2000]: LA–ICPMS analyses for these samples are reported herein and are shown on this diagram. Samples reported by others are as follows: 1 = *Martin et al.* [2005]; 2 = *McQuarrie et al.* [2008]; 3 = *Martin et al.* [2011]; 4 = *Kohn et al.* [2010]. The lower curve is a composite of all analyses from lower Lesser Himalayan strata. Note that results from upper Lesser Himalayan strata (Cambrian through Cretaceous age) are shown with data from correlative rocks of the Tethyan Sequence (Figure 7).

uncertainty (internal error only) as a normal distribution, and sum all ages from a sample into a single curve. Composite age probability plots are made from an in-house Excel program (available from http://www.laserchron.org) that normalizes each curve according to the number of constituent analyses, such that each curve contains the same area, and then stacks the probability curves. In some cases, where noted, the height of an age-distribution curve has been modified for scaling purposes.

[38] Maximum depositional ages are reported for some strata using the youngest single grain as well as the more robust criteria of using the youngest peak in age probability that is defined by at least three overlapping ages. As described by *Dickinson and Gehrels* [2009], the youngest single grain commonly yields a maximum depositional age that may be younger than the true depositional age (due to Pb loss or simply due to measurement statistics), whereas

the age-probability peak defined by at least three overlapping analyses is a more robust determination of maximum depositional age.

## 4. Samples and Results

[39] We have attempted to collect samples from the main stratigraphic horizons in each of the assemblages exposed along a broad transect across the Himalaya and Tibet Plateau, from the Indian craton on the south to the Tarim/North China craton on the north (Figure 1). The sample coverage is described briefly below and shown on Figures 1–4, and location information for each sample for which new information is presented is provided in Table 1. The detrital zircon data are reported in Tables S1–S8, and concordia plots of all new analyses are presented in Figures S1–S7. Normalized probability plots for each crustal fragment are
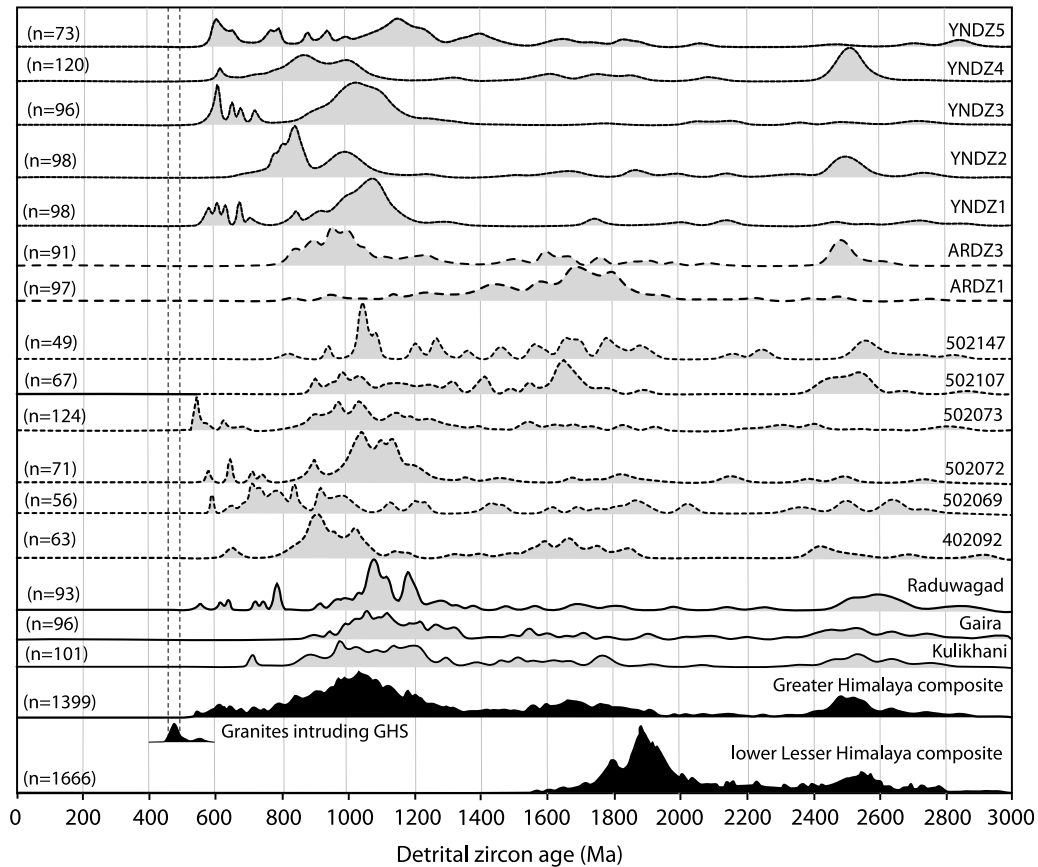
**Figure 6.** Normalized probability plots for Greater Himalayan strata. Two samples (ARDZ1, ARDZ3) were previously analyzed with ID–TIMS by *DeCelles et al.* [2000], and have been reanalyzed herein by LA–ICPMS. Six samples (502147, 502107, 502073, 502072, 502069, and 402092) were reported by *Martin et al.* [2005], and three samples from frontal thrust sheets (Raduwagad, Gaira, Kulikhani) were reported by *Gehrels et al.* [2006a, 2006b]. The lower curves are composites of all analyses from lower Lesser Himalayan and Greater Himalayan strata. Ages of granites intruding Greater Himalayan strata are from compilation of *Cawood et al.* [2007].

presented on Figures 5–11 and summarized on Figure 12. Provenance interpretations are presented on Figures 13 and 14.

### 4.1. Lower Lesser Himalayan Strata (LHS)

[40] Our samples include one or more from each of the classic lower Lesser Himalayan units of Nepal in the central Himalaya, including the Kuncha, Kushma, Fagfog, Sangram, Lakhaparta, and Syangja formations, all of which are Early to Middle Proterozoic in age (Figure 4) [*DeCelles et al.*, 2000, 2001; *Martin et al.*, 2011]. ID–TIMS analyses from these strata were reported by *DeCelles et al.* [2000]; we herein report LA–ICPMS analyses from the same samples (Figure S1 and Table S1). Other detrital zircon data sets from Paleo- and Mesoproterozoic strata from the Lesser Himalaya have been reported from Nepal [*Martin et al.*, 2005, 2011; *Kohn et al.*, 2010] and Bhutan [*McQuarrie et al.*, 2008].

[41] All available data from these lower Lesser Himalayan strata are shown on Figure 5 and reported in Figure S1 and Table S1. In all samples, detrital zircon grains are older than 1.4 Ga, with dominant ages between 1.7 and 2.0 Ga and subordinate ages between 2.4 and 2.8 Ga (Table S1). Grains of these ages were most likely derived from igneous rocks

that are closely associated with Lesser Himalayan strata (e.g., ~1.82 Ga Ulleri orthogneiss) as well as from broader regions of the northern Indian craton (see *Kohn et al.* [2010] for a recent summary of the origin and provenance of lower Lesser Himalayan strata). The younging of peak ages and minimum ages upsection in lower Lesser Himalayan strata (Figure 5) may reflect a combination of evolving sources through time and decreasing depositional age. The composite curve for lower LHS strata (Figure 5) is used in this study primarily as a reference for the ages of grains that were derived from the northern Indian craton.

[42] The detrital zircon ages available from upper Lesser Himalayan strata, of Neoproterozoic through Cretaceous age, are discussed with ages from Tethyan strata given that the units are directly correlative.

### 4.2. Greater Himalayan Sequence (GHS)

[43] Detrital zircon U-Pb data have been reported by previous workers, as follows: *Parrish and Hodges* [1996] reported eight ID–TIMS analyses from metasedimentary rocks collected from central Nepal; *DeCelles et al.* [2000] reported ID–TIMS data from two samples collected from eastern Nepal (reanalyzed in this study by LA–ICPMS);
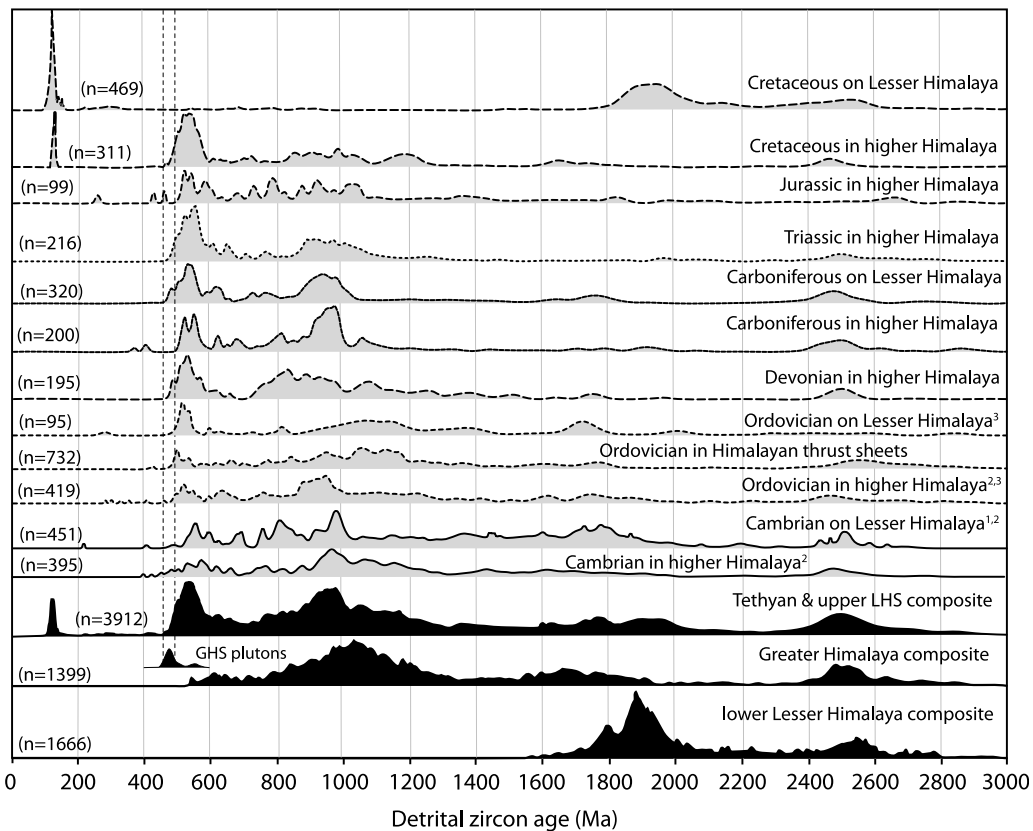
**Figure 7.** Normalized probability plots for Tethyan strata and correlative upper Lesser Himalayan strata (in the frontal Himalaya). Because of the large number of samples, ages from generally coeval strata have been combined into composite age distributions. The ages from "Cambrian on Lesser Himalaya" are from *Myrow et al.* [2003, 2010][1,2], and ages from "Ordovician on Lesser Himalaya are from *McQuarrie et al.* [2008][3]. Samples in "Ordovician in Higher Himalaya" are from this study as well as *McQuarrie et al.* [2008][3] and *Myrow et al.* [2010][2]. Some of the Cretaceous samples were previously analyzed by ID–TIMS and reported by *DeCelles et al.* [2000]: the ages reported herein are from LA–ICPMS analyses of the same samples. Composite curves for Greater Himalayan and lower Lesser Himalayan strata are shown for reference. Ages of granites intruding Greater Himalayan strata are from compilation of *Cawood et al.* [2007].

*Martin et al.* [2005] reported LA–ICPMS data from six samples from central Nepal; *Gehrels et al.* [2006a] reported LA–ICPMS data from three samples collected from lower-grade equivalents of GHS rocks in thrust sheets of the frontal Himalaya in central Nepal; and *Myrow et al.* [2009] reported detrital zircon data from sandstones in the Mount Everest region of southern Tibet that are found below the South Tibetan Detachment System and may accordingly belong to the Greater Himalayan sequence. Because the latter rocks are much lower in metamorphic grade and degree of deformation than typical Greater Himalayan rocks, the ages from these strata are of uncertain significance relative to other Greater Himalayan rocks and are accordingly not considered further. Herein we report analyses from five additional samples that were collected along a traverse across the Greater Himalayan sequence in central Nepal (Figure 2). Data from all of these studies are reported in Figure S2 and Table S2.

[44] Age-probability curves (Figure 6) indicate that all GHS samples have ages of 800–1200 Ma, 1.6–1.9 Ga, and 2.4–2.7 Ga, and that about half of the samples contain Neoproterozoic (540–750 Ma) grains. This suggests that all GHS protoliths are younger than 800–1200 Ma, as suggested by *Parrish and Hodges* [1996], and that some may be as young as 540–750 Ma. A comparison of samples YNDZ1–5 provides an opportunity to evaluate differences in provenance and maximum depositional age across a ~6-km-thick sequence of GHS strata. Unfortunately no simple pattern appears, with the youngest grains in the structurally lowest sample, and the only sample without 540–750 Ma grains found at structurally higher levels. It is uncertain whether these variations are due to structural imbrication (inversion?) or to a change in provenance through time.

[45] The minimum age of deposition of GHS protoliths is constrained by granitic bodies (now mainly orthogneisses) that range in age from 470 to 550 Ma (most between 470 and 490 Ma [*Cawood et al.*, 2007]). For comparison with younger strata, the probability distribution of these igneous ages is shown on Figure 6.
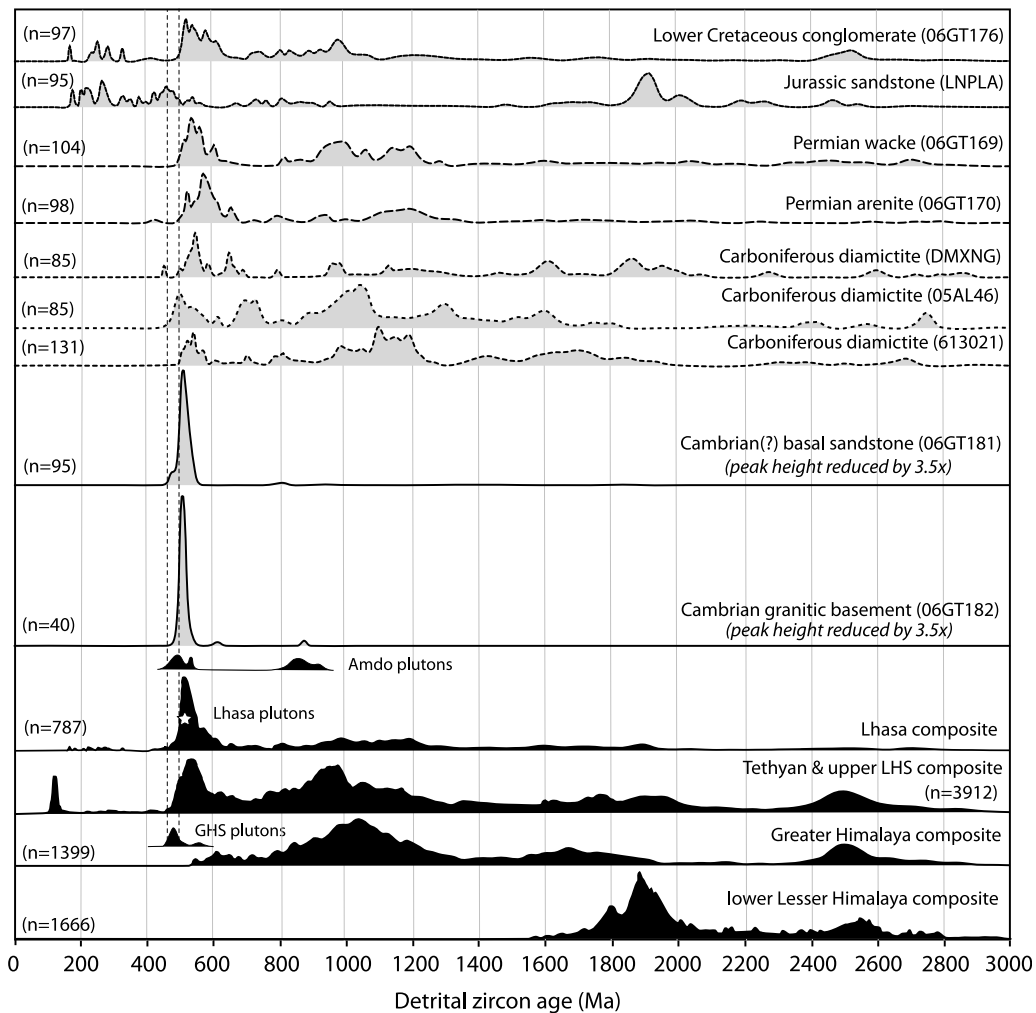
**Figure 8.** Normalized probability plots for strata from the Lhasa terrane. The age distribution from a granite body underlying the Cambrian strata is also shown. Two samples (DMXNG and LNPLA) were analyzed and reported by *Leier et al.* [2007]. Composite curves for Greater Himalayan, lower Lesser Himalayan, and Tethyan/upper LHS strata are shown for reference. Ages of granites intruding Greater Himalayan strata are from compilation of *Cawood et al.* [2007].

[46] The full set of ages available from the GHS is compiled into a single age distribution on Figure 6. This age distribution is not similar to available ages from lower Lesser Himalayan strata, also shown on Figure 6, which suggests that GHS protoliths were not shed directly from the local Indian craton or recycled from the lower LHS platformal cover [e.g., *Parrish and Hodges*, 1996]. As suggested by *DeCelles et al.* [2000], and discussed in detail by *Myrow et al.* [2010], such ages are more consistent with derivation from portions of Gondwana that contain both Pan-African (Neoproterozoic) and Grenville-age (Mesoproterozoic) igneous rocks, with the East African orogen the most likely specific source (Figures 6, 13a, and 13b). It is also possible that much of the detritus was derived from the Eastern Ghats, Pinjara and Wilkes–Frasier/Rayner/Maud orogens in eastern India, Western Australia, and Antarctica [*Yoshida and Upreti*, 2006; *Cawood et al.*, 2007]. The presence of Archean and Paleoproterozoic grains in GHS samples likely records sedimentary transport across the Indian craton [e.g., *Myrow et al.*, 2010].

### 4.3. Tethyan and Upper Lesser Himalayan Strata

[47] Thirteen samples have been analyzed by LA–ICPMS from the main sequence of Tethyan strata in the higher Himalaya (Table S3 and Figure S3). Our samples are from Cambrian (?), Ordovician, Devonian, Triassic, Jurassic, and Cretaceous strata, and all are from the Kali Gandaki and Marsyangdi drainages of central Nepal (Figure 2). *Myrow et al.* [2010] and *McQuarrie et al.* [2008] have reported U-Pb ages of detrital zircons from Cambrian and Ordovician Tethyan strata from northern India, Bhutan, and Pakistan, which are also included in Table S3 for reference.

[48] Detrital zircons have also been analyzed from Ordovician (?) strata that rest unconformably on Greater Himalayan rocks in thrust sheets of the frontal Himalaya in Nepal (Figure 2). Two of these Ordovician (?) samples from central and western Nepal were originally analyzed by ID–TIMS [*DeCelles et al.*, 2000] and have been reanalyzed by LA–ICPMS (data reported herein). Five samples analyzed by LA–ICPMS were reported by *Gehrels et al.* [2006a,
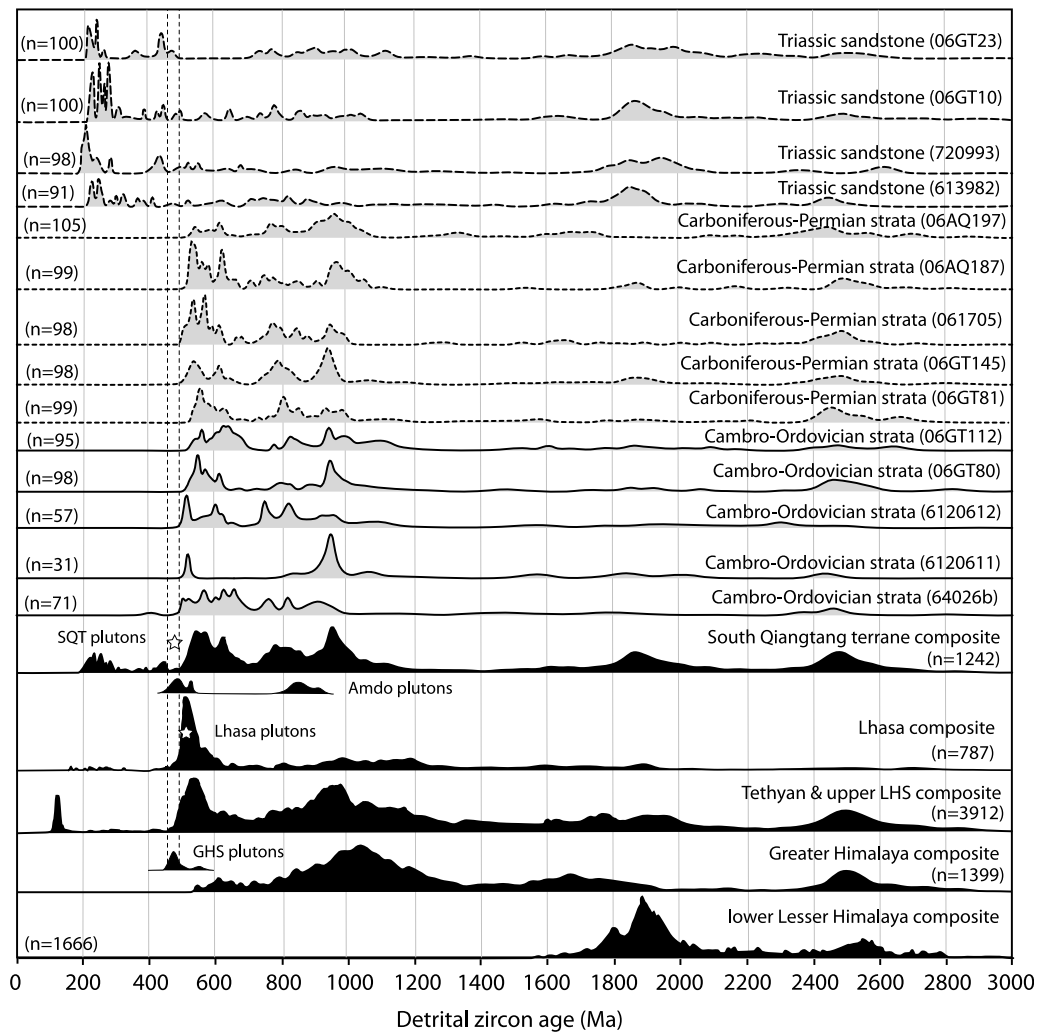
**Figure 9.** Normalized probability plots for strata from the southern Qiangtang terrane. All samples of Cambro–Ordovician strata and two samples of Carboniferous–Permian strata (06GT145, 06GT81) are from *Pullen et al.* [2010]. Composite curves for Greater Himalayan, lower Lesser Himalayan, Tethyan/ upper LHS, and Lhasa strata are shown for reference. Also shown are approximate ages of granites intruding Greater Himalayan strata (from compilation of *Cawood et al.* [2007], Lhasa terrane [this study], and the southern Qiangtang terrane [*Pullen et al.*, 2010]).

2006b], and one additional sample (Mirul Formation) analyzed by LA–ICPMS is reported herein.

[49] We also include in this section the results from Cambrian strata of the upper Lesser Himalayan Sequence in India and Bhutan [*Myrow et al.*, 2010], Ordovician (?) strata in Bhutan [*McQuarrie et al.*, 2008], and upper Paleozoic through Tertiary strata of the Gondwanan Series in Nepal [*Sakai*, 1991; *Upreti*, 1999]. Results from these strata are included herein, rather than with the discussion of lower Lesser Himalayan stratigraphy, because they are clearly correlative with Tethyan strata in the higher Himalaya (Figure 4) [*Upreti*, 1999; *Gehrels et al.*, 2003; *Myrow et al.*, 2010]. *DeCelles et al.* [2004] reported U-Pb ID–TIMS ages from three samples of Cretaceous strata from the Gondwana Series in central Nepal (Amile, db-02-21ex-1 and db-02-21LX of Table 1). We have generated additional LA–ICPMS ages for these samples, and have also analyzed

three Carboniferous–Permian samples that were collected from central Nepal (Figure 2).

[50] Detrital zircon samples have also been analyzed from upper Lesser Himalayan strata in northern India by *Célérier et al.* [2009]. Results from these samples are not included in this compilation, however, because the U-Pb geochronologic data have not reported.

[51] The Tethyan and correlative upper Lesser Himalayan samples reveal a surprising degree of similarity in strata extending from Cambrian through Cretaceous age (Figure 7). Except for Cretaceous strata of the Gondwana Series (in the frontal Himalaya), all of the units are dominated by age groups of approximately 480–570 Ma, 750–1200 Ma, and 2430–2560 Ma. Our preferred interpretations for provenance of the Tethyan and upper Lesser Himalayan strata are as follows:

[52] 1. Cambrian: derivation from broad regions of Gondwana, mainly the East African orogen [e.g., *DeCelles*
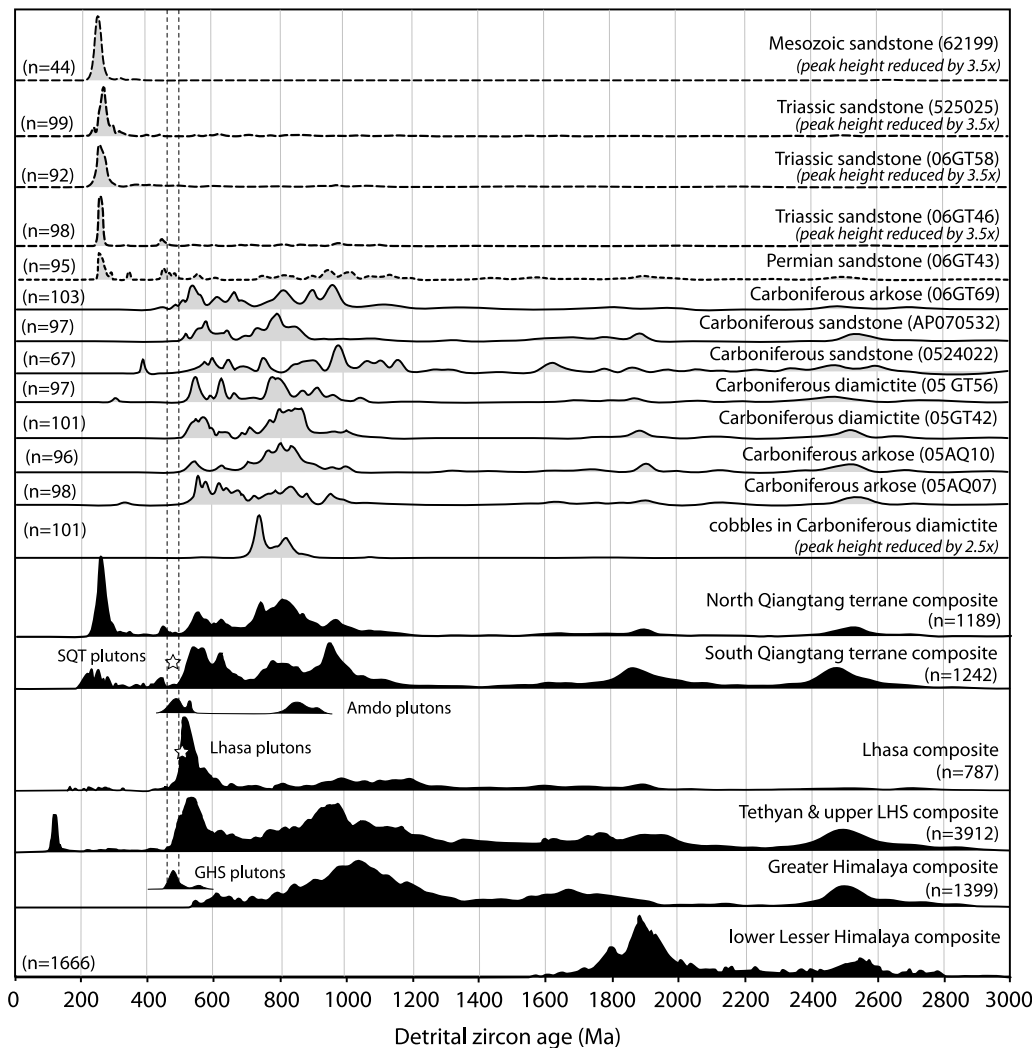
**Figure 10.** Normalized probability plots for strata from the northern Qiangtang terrane. All samples are reported herein for the first time. Composite curves for Greater Himalayan, lower Lesser Himalayan, Tethyan/upper LHS, Lhasa, and South Qiangtang strata are shown for reference. Also shown are approximate ages of granites intruding Greater Himalayan strata (from compilation of *Cawood et al.* [2007], Lhasa terrane [this study], and the southern Qiangtang terrane [*Pullen et al.*, 2010]).

*et al.*, 2000] but also from the Ross–Delamerian orogen of Australia and Antarctica [*Myrow et al.*, 2010] (Figure 13a).

[53] 2. Ordovician: Continued derivation from the East African and Ross–Delamerian orogens [*DeCelles et al.*, 2000; *Myrow et al.*, 2010], with possible input from uplifted Greater Himalayan rocks and Cambro–Ordovician granites intruding the Greater Himalayan sequence [*McQuarrie et al.*, 2008] (Figure 13b). Possible derivation from the Greater Himalayan sequence is based on the increase in abundance of 1.0–1.2 Ga ages, which matches the higher proportions found in Greater Himalayan samples (Figure 7), and the shift to slightly younger Cambro–Ordovician age peaks in the Ordovician strata. The presence of coarse conglomerates of Ordovician age in the Tethyan sequence [e.g., *Garzanti et al.*, 1986; *Gehrels et al.*, 2006b] also records the presence of local uplifts, as opposed to derivation entirely from distant sources.

[54] 3. Silurian through Jurassic: these strata were apparently shed from broader regions of Gondwana, rather than predominantly Greater Himalayan rocks and their Cambro–Ordovician plutons, as most Cambro–Ordovician ages shift back to pre-520 Ma, and most mid-Proterozoic ages shift back to <1.0 Ga. During Carboniferous time, when Tethyan strata are mainly glaciogenic diamictites, most detritus was presumably carried from the polar ice cap, which was centered on Antarctica and southern India [*Blakey*, 2008] (Figure 13c–13g).

[55] 4. Cretaceous: Cretaceous strata in the frontal Himalaya yield detrital zircon grains that were likely shed from lower LHS strata or underlying crystalline rocks of the Indian craton [*DeCelles et al.*, 2004], whereas Cretaceous strata in the higher Himalaya appear to also include detritus derived from underlying strata of the upper LHS, Tethyan, and/or Greater Himalayan sequences (Figure 6). Cretaceous zircons in both sets of units are interpreted to have been derived from volcanic rocks that *Dürr and Gibling* [1994], *Garzanti* [1999], *DeCelles et al.* [2004], and *Hu*
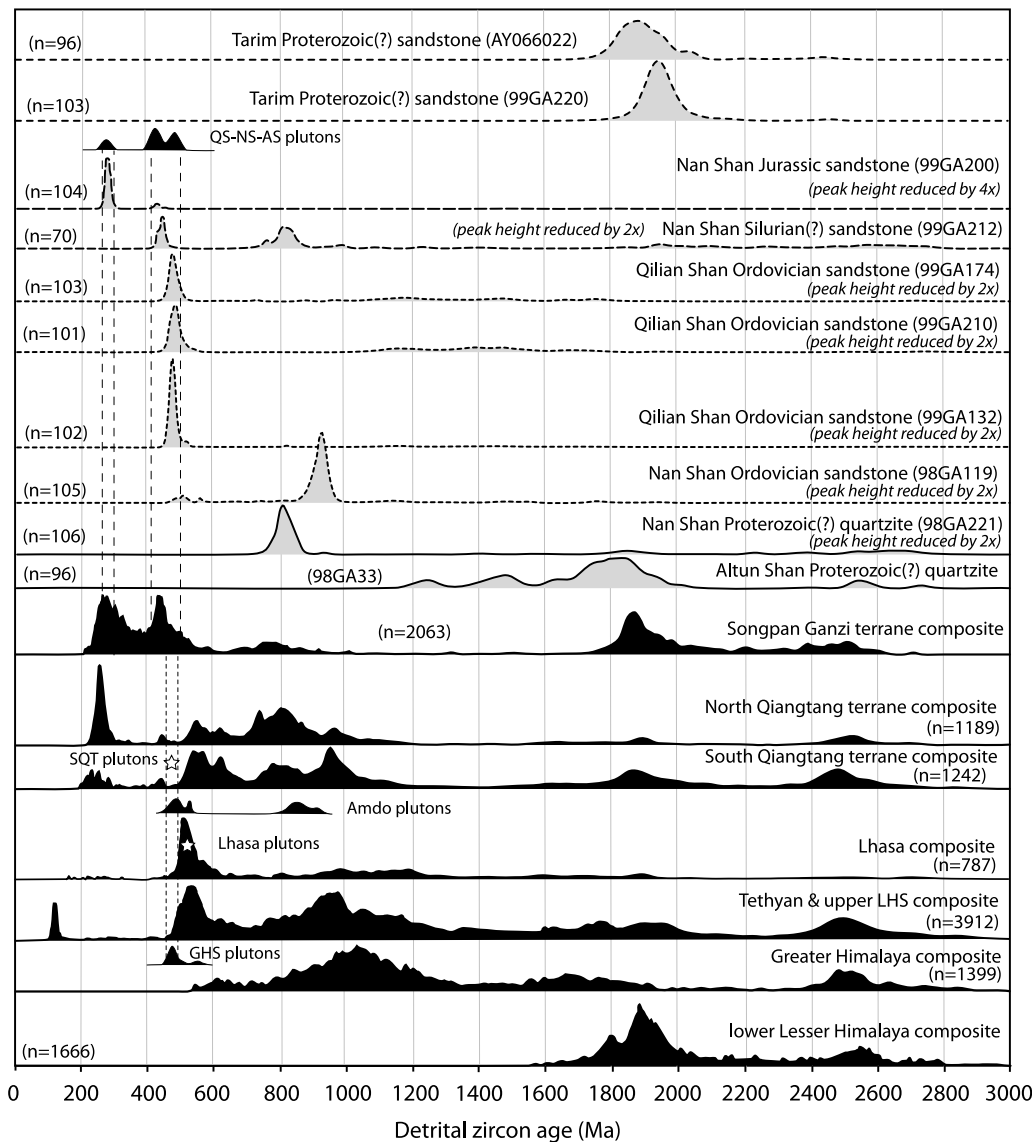
**Figure 11.** Normalized probability plots for strata from the Songpan Ganzi terrane [from *Weislogel et al.*, 2006], the Nan Shan–Qilian Shan–Altun Shan terrane, and Tarim craton. The latter samples were originally analyzed by ID–TIMS by *Gehrels and Yin* [2003a] and have been re-analyzed by LA–ICPMS herein. Composite curves for Greater Himalayan, lower Lesser Himalayan, Tethyan/upper LHS, Lhasa, South Qiangtang, and North Qiangtang strata are shown for reference. Also shown are approximate ages of granites intruding Greater Himalayan strata (from compilation of *Cawood et al.* [2007]), Lhasa terrane [this study], southern Qiangtang terrane [*Pullen et al.*, 2010], and Nan Shan–Qilian Shan–Altun Shan terrane [*Gehrels and Yin*, 2003b]).

*et al.* [2008, 2009] attribute to Cretaceous rifting of India from Gondwana (Figure 13h).

## 4.4. Lhasa Terrane

[56] Our samples were collected in the central portion of the Lhasa terrane (Figure 3) from a sequence of Paleozoic strata reported by *Pan et al.* [2004]. We also analyzed zircons from a hypabyssal granite body that is overlain unconformably by these strata, and from strata mapped by *Pan et al.* [2004] as Jurassic or Lower Cretaceous.

[57] The underlying granite body is fine-grained and quartz-porphyritic, and yielded zircons with typical igneous

characteristics (shape, color, U concentration, U/Th, etc.). Two analyses yield $^{206}Pb/^{238}U$ ages of ~613 Ma and ~875 Ma, presumably of inherited zircon, whereas all other analyses define a cluster with a weighted mean age of 510.4 ± 6.5 Ma (2-sigma, MSWD = 0.8) (Table S4 and Figure S4). This age is consistent with ages of crystalline rocks of Amdo basement [*Guynn et al.*, 2006, 2011], as shown on Figure 8.

[58] The overlying Paleozoic strata include a 5-m-thick basal conglomerate that rests directly on the Cambrian granite. These conglomeratic strata grade upward into well-bedded sandstone, which is overlain by dark mudstone and

**Table 1.** Information About U-Pb Geochronologic Samples for Which New Geochronologic Data Are Presented[a]

| Sample | Depositional Age | Rock Type | Elevation (m) | Latitude | Longitude | Reference |
|---|---|---|---|---|---|---|
| *Lower Lesser Himalayan Strata* | | | | | | |
| ARDZ2 | Proterozoic | Quartzite | | 27°24'36.3"N | 87°6'42.0"E | *DeCelles et al.* [2000] |
| ARDZ5 | Proterozoic | Quartzite | | 27°22'40.0"N | 87°15'48.0"E | *DeCelles et al.* [2000] |
| Budar | Proterozoic | Quartzite | | | | *DeCelles et al.* [2000] |
| Kushma | Proterozoic | Quartzite | | 29°40'59.8"N | 81°20'03.3"E | *DeCelles et al.* [2000] |
| Lakhaparta | Proterozoic | Quartzite | | 29°29'02.4"N | 81°3'06.0"E | *DeCelles et al.* [2000] |
| Sangram | Proterozoic | Quartzite | | 29°24'26.3"N | 80°37'41.4"E | *DeCelles et al.* [2000] |
| Syangia | Proterozoic | Quartzite | | 29°29'29.2"N | 81°4'35.6"E | *DeCelles et al.* [2000] |
| Fagfog | Proterozoic | Quartzite | 1151 | 28°28'58.2"E | 83°38'42.5"E | This study |
| *Upper Lesser Himalaya Strata (Gondwana Sequence)* | | | | | | |
| Lower Sisne | Carboniferous | Pebbly greenish medium-grained arkosic sandstone | 638 | 27°47'24.9"N | 83°32'33.8"E | This report |
| Middle Sisne | Carboniferous | Pebbly greenish coarse-grained arkosic sandstone | 741 | 27°47'34.5"N | 83°32'34.7"E | This report |
| Upper Sisne | Carboniferous | Pebbly greenish medium-grained arkosic sandstone | 625 | 27°47'38.0"N | 83°32'40.1"E | This report |
| Taltung | Cretaceous | Volcanic-rich sandstone | 609 | 27°47'41.7"N | 83°31'54.9" | This report |
| Charchare | Cretaceous | Pebbly volcanic-rich sandstone | 649 | 27°47'40.8"N | 83°31'54.1"E | This report |
| Amile | Cretaceous | | | | | *DeCelles et al.* [2004] |
| db-02-21ex-1 | Cretaceous | | | | | *DeCelles et al.* [2004] |
| db-02-21LX | Cretaceous | | | | | *DeCelles et al.* [2004] |
| *Greater Himalayan Rocks* | | | | | | |
| YNDZ1 | Pre-Ordovician (?) | Quartzite | 1181 | 28°22'03.1"N | 84°24'17.6"E | This report |
| YNDZ2 | Pre-Ordovician (?) | Quartzite | 1277 | 28°23'56.7"N | 84°24'27.5"E | This report |
| YNDZ3 | Pre-Ordovician (?) | Quartzite | 1603 | 28°25'11.5"N | 84°24'15.2"E | This report |
| YNDZ4 | Pre-Ordovician (?) | Quartzite | 1673 | 28°28'27.3"N | 84°22'28.7"E | This report |
| YNDZ5 | Pre-Ordovician (?) | Quartzite | 1698 | 28°31'00.9"N | 84°21'27.3"E | This report |
| ARDZ1 | Pre-Ordovician (?) | Quartzite | | 26°59'13.7"N | 87°10'46.4"E | *DeCelles et al.* [2000] |
| ARDZ3 | Pre-Ordovician (?) | Quartzite | | 27°24'36.3"N | 87°06'42.0"E | *DeCelles et al.* [2000] |
| *Tethyan Strata (Higher Himalaya)* | | | | | | |
| Amapuma | Cambrian (?) | Fine-grained quartzite | 2581 | 28°43'26.9"N | 83°38'55.2"E | This report |
| NFDZ1 | Ordovician | Fine-grained arkosic quartzite | 3373 | 28°38'16.3"N | 84°07'46.8"E | This report |
| NFDZ3 | Ordovician | Fine-grained arkosic quartzite | 2696 | 28°45'12.9"N | 83°41'45.2"E | This report |
| Tilicho Pass 1 | Devonian | Coarse micaceous arkose | 3592 | 28°35'40.5"N | 84°07'11.2"E | This report |
| Tilicho Pass 2 | Devonian | Coarse micaceous arkose | 2699 | 28°45'02.0"N | 83°41'31.9"E | This report |
| Thini Chu #1 | Carboniferous | Pebbly arkosic sandstone | 3241 | 28°45'55.1"N | 83°44'31.2"E | This report |
| Thini Chu #2 | Carboniferous | Medium-grained sandstone | 3376 | 28°46'05.1"N | 83°44'30.8"E | This report |
| FDQ #1 | Triassic | Fine-grained sandstone | | 28°47'27.8"N | 83°45'35.9"E | This report |
| FDQ #2 | Triassic | Medium-grained micaeous arkosic sandstone | 3342 | 28°46'34.3"N | 83°44'41.4"E | This report |
| Laptal | Jurassic | Fine-grained calcareous sandstone | 2808 | 28°48'57.7"N | 83°46'08.9"E | This report |
| Chukh | Cretaceous | Medium-grained sandstone | | 28°48'53.3"N | 83°51'29.5"E | This report |
| Dangarzhong | Cretaceous | Medium-grained quartz arenite | 2829 | 28°50'14.2"N | 83°46'54.1"E | This report |
| Kagbeni | Cretaceous | Coarse-grained volcanic-rich arkosic sandstone | 2828 | 28°50'16.9"N | 83°46'57.2"E | This report |
| *Tethyan Strata (Thrust Sheets)* | | | | | | |
| upper Damgad sandstone | Ordovician | Medium-grained arkosic sandstone | | 29°18'17.7"N | 80°44'15.7"E | *DeCelles et al.* [2000] |
| Mirul | Ordovician (?) | Medium-grained arkosic sandstone | 1429 | 28°31'54.9"N | 82°31'54.9"E | This report |

**Table 1.** (continued)

| Sample | Depositional Age | Rock Type | Elevation (m) | Latitude | Longitude | Reference |
|---|---|---|---|---|---|---|
| *Lhasa Terrane* | | | | | | |
| 06GT182 | Precambrian (?) | Quartz-porphyry granite below basal conglomerate | 4778 | 30°51'02.7"N | 89°17'51.3"E | This report |
| 06GT181 | Cambrian (?) | Pebbly sandstone | 4773 | 30°51'27.3"N | 89°17'32.4"E | This report |
| 6-13-02-1 | Carboniferous | Medium-grained sandstone | 4354 | 30°27'56.1"N | 91°01'19.8"E | This report |
| 05AL46 | Carboniferous | Metagreywacke | 5013 | 30°38'36.4"N | 91°06'13.6"E | This report |
| 06GT170 | Permian | Quartz arenite | 4874 | 31°11'28.3"N | 88°45'30.0"E | This report |
| 06GT169 | Permian | Volcanic-lithic sandstone | 4783 | 31°11'23.0"N | 88°45'23.0"E | This report |
| 06GT176 | Jurassic (?) | Quartz arenite | 4788 | 31°29'53.0"N | 89°13'44.2"E | This report |
| *Southern Qiangtang* | | | | | | |
| 061705 | Carboniferous | Arkosic quartzite | 5080 | 33°03'424.1"N | 84°16'19.9"E | This report |
| 06AQ187 | Carboniferous | Medium arkose | 5006 | 33°25'19.3"N | 85°59'04.4"E | This report |
| 06AQ197 | Carboniferous | Quartzite | 4820 | 33°26'57.5"N | 85°49'39.1"E | This report |
| 613982 | Triassic | Medium-grained sandstone | 4925 | 32°56'46.2"N | 84°06'17.5"E | This report |
| 720993 | Triassic | Sandstone | | 32°30'14.4"N | 85°44'55.2"E | This report |
| 06GT23 | Triassic | Sandstone | 4873 | 32°26'47.2"N | 86°38'09.5"E | This report |
| 06GT10 | Triassic | Quartz arenite | 4815 | 32°26'36.4"N | 86°38'18.0"E | This report |
| *Northern Qiangtang* | | | | | | |
| 05AQ07 | Carboniferous-Permian | Coarse arkose in diamictite | 5201 | 34°12'17.0"N | 82°55'46.7"E | This report |
| 05AQ10 | Carboniferous-Permian | Coarse arkose in diamictite | 5174 | 34°13'04.6"N | 82°55'41.2"E | This report |
| 05GT42 | Carboniferous-Permian | Pebbly sand in diamictite | 5280 | 34°09'54.8"N | 82°54'34.8"E | This report |
| 05GT56 | Carboniferous-Permian | Arkose in diamictite | 5305 | 34°10'13.9"N | 82°55'00.1"E | This report |
| 5-24-02-2 | Carboniferous | Coarse-grained arkosic sandstone | 5256 | 33°29'20.4"N | 86°50'37.6"E | This report |
| AP0703052 | Carboniferous-Permian | Arkose | | 34°12'25.9"N | 82°56'00.8"E | This report |
| 06GT69 | Carboniferous-Permian (?) | Red sandstone | 4732 | 33°37'26.2"N | 85°49'20.6"E | This report |
| 06GT43 | Permian | Greenish sandstone | 4782 | 33°39'52.1"N | 86°50'37.4"E | This report |
| 06GT46 | Triassic | Sandstone | 4881 | 33°39'36.5"N | 86°50'15.0"E | This report |
| 06GT58 | Triassic | Fine sandstone | 4831 | 33°38'45.5"N | 86°50'39.8"E | This report |
| 5-25-02-5 | Triassic | Medium-grained sandstone | 4802 | 33°38'55.7"N | 86°50'55.9"E | This report |
| 621991 | Mesozoic | Feldspathic sandstone | 4905 | 33°28'59.0"N | 87°27'05.6"E | This report |
| 619051 | Carboniferous-Permian | Diamictite cobbles | 5104 | 34°03'06.3"N | 84°47'58.4"E | This report |
| *Qilian Shan–Nan Shan–Altun Shan* | | | | | | |
| 98GA33 | Proterozoic (?) | Quartzite | | 38°47'04.0"N | 91°01'22.9"E | *Gehrels et al.* [2003] |
| 98GA221 | Proterozoic (?) | metaturbidites | | 39°13'25.3"N | 94°17'40.2"E | *Gehrels et al.* [2003] |
| 98GA119 | Ordovician | Volcanic wacke | | 39°02'47.3"N | 95°33'35.2"E | *Gehrels et al.* [2003] |
| 99GA132 | Ordovician | Volcanic wacke | | 39°28'35.9"N | 95°48'56.0"E | *Gehrels et al.* [2003] |
| 99GA210 | Ordovician | Recycled orogenic sandstone | | 39°31'27.9"N | 96°08'56.1"E | *Gehrels et al.* [2003] |
| 99GA174 | Ordovician | Recycled orogenic sandstone | | 39°06'34.0"N | 91°27'49.8"E | *Gehrels et al.* [2003] |
| 99GA212 | Silurian (?) | Recycled orogenic sandstone | | 38°02'30.1"N | 95°09'16.9"E | *Gehrels et al.* [2003] |
| 99GA200 | Jurassic | Recycled orogenic sandstone | | 40°03'11.0"N | 97°23'01.3"E | *Gehrels et al.* [2003] |
| *Tarim Craton* | | | | | | |
| 98GA220 | Proterozoic (?) | quartzite | | 39°17'15.4"N | 93°00'08.4"E | *Gehrels et al.* [2003] |
| AY66022 | Proterozoic (?) | Quartzite | | | | |

aDatum for locations is WGS 84. Depositional ages have been revised in some cases according to detrital zircon ages.
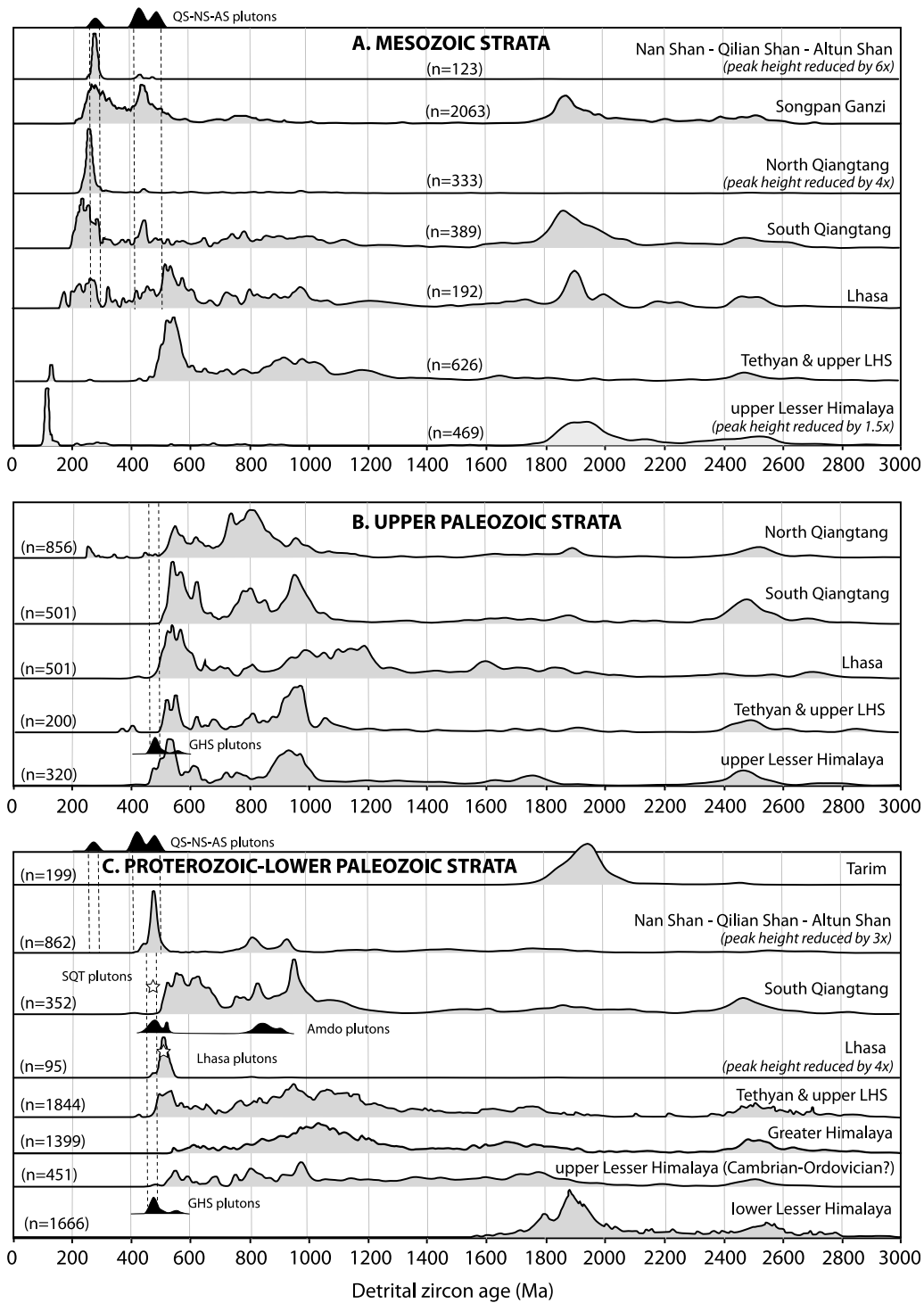
**Figure 12.** Normalized probability plots for strata of various ages in the terranes/assemblages analyzed. The number of constituent analyses is shown for each set of ages. (a) Strata of Proterozoic through Devonian age. (b) Strata of late Paleozoic age. (c) Strata of Mesozoic age. Also shown are approximate ages of granites intruding Greater Himalayan strata (from compilation of *Cawood et al.* [2007], Lhasa terrane [this study], southern Qiangtang terrane [*Pullen et al.*, 2010], and Nan Shan–Qilian Shan–Altun Shan terrane [*Gehrels and Yin*, 2003b]).

carbonate that *Pan et al.* [2004] portray as Ordovician in age. Cobbles in the conglomerate range up to 30 cm in diameter and are interpreted to have been derived from the underlying granite based on petrographic similarities.

Zircons in a sandstone from immediately above the basal conglomerate yield mainly Cambrian ages (age peak at 511 Ma), with six additional ages of 790 to 1840 Ma (Table S4 and Figure S4). We interpret these basal strata as
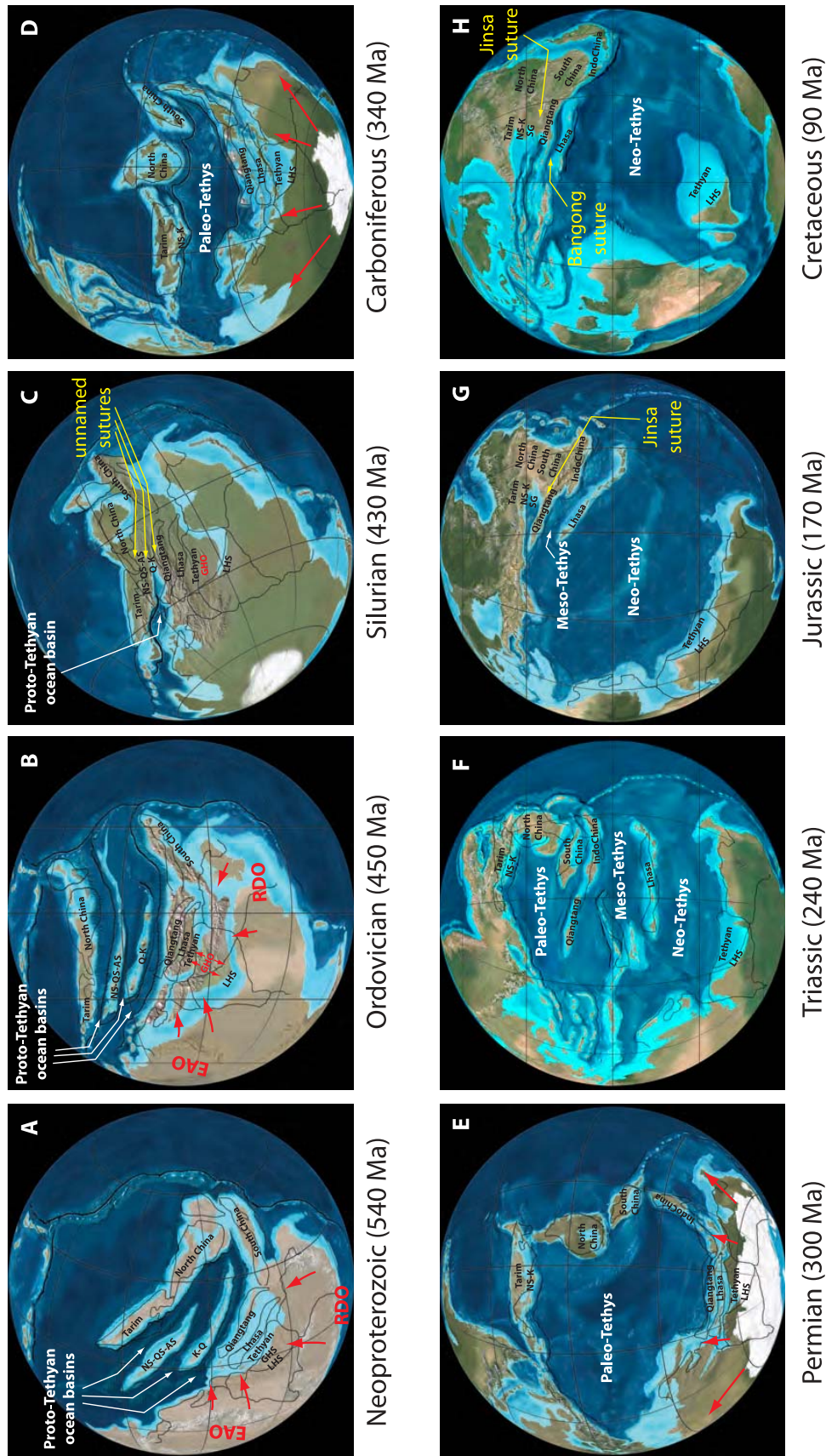
**Figure 13.** (a–h) Paleogeographic maps showing the evolution of the terranes and assemblages in the Tibet–Himalayan orogen. Maps are adapted from *Dewey et al.* [1988], *Hsü et al.* [1995], *Şengör and Natal'in* [1996a], *Metcalfe* [1996], *Yin and Nie* [1996], *Yin and Harrison* [2000], *Heubeck* [2001], *Stampfli and Borel* [2002], *Blakey* [2008], and *Torsvik and Cocks* [2009]. Red lines show interpreted provenance. LHS = Lesser Himalayan Sequence, GHS = Greater Himalayan Sequence, Q–K = Qaidam–Kunlun terrane, NS–QS–AS = Nan Shan–Qilian Shan–Altun Shan terrane, RDO = Ross–Delamerian orogen. EAO = East African orogen. GHO = Greater Himalayan orogen.
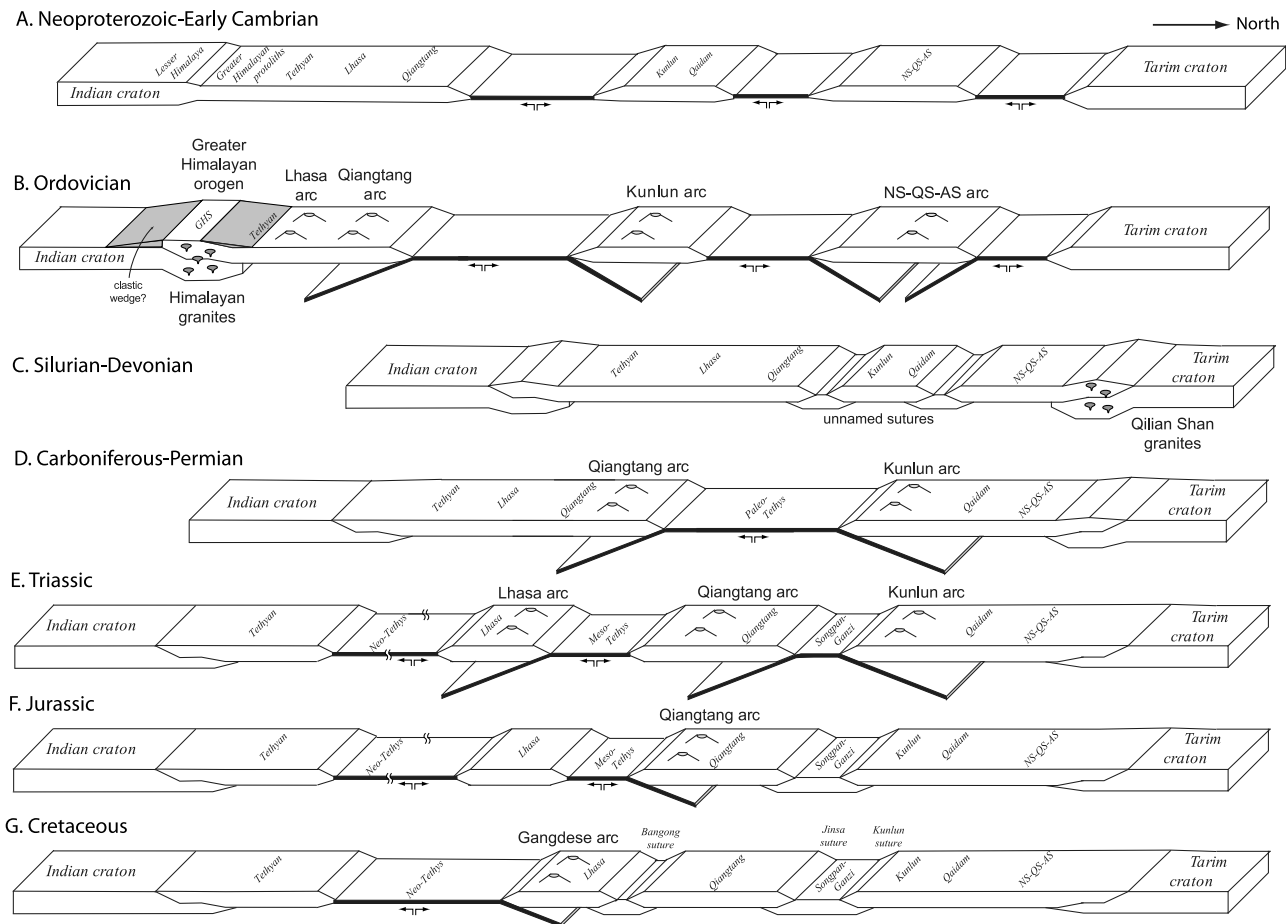
**Figure 14.** (a–g) Schematic diagrams showing preferred tectonic reconstructions based on previous syntheses (cited in the text and Figure 13) complemented by the detrital zircon data presented herein. Format adapted from *Yin and Harrison* [2000].

Cambrian in age (Figure 4), although they may instead be part of the overlying Ordovician section. Unfortunately, a sample of Ordovician mudstone with fine-grained sandstone interbeds failed to yield zircons.

[59] One sample of Carboniferous sandstone with diamictite pebbles (sample DMXNG) was previously analyzed from the eastern Lhasa terrane (Figures 3 and 4) by *Leier et al.* [2007]. Two additional samples of Carboniferous age have been analyzed from the Nyainqentanglha area as part of this study (Figures 3 and 4). These three samples collectively yield predominantly Cambrian-age zircons (age peaks at 501, 511, and 524 Ma) as well as numerous zircons of Proterozoic and Archean age (major age peaks at 670–760, 780–840, 940–1240, 1280–1340, 1550–1940, and 2360–2790 Ma) (Figure 8, Table S4, and Figure S4).

[60] Two samples of Permian age were collected from the north-central part of the terrane [*Pan et al.*, 2004]. The youngest and most abundant ages are represented by age peaks at 514, 524, 560, and 571 Ma, and there are scattered ages at 650–690, 790–840, 920–1080, 1110–1350, and 1930–2840 Ma (Figure 8, Table S4, and Figure S4). Although there is a significant volcanic-lithic component to most Permian sandstone horizons in the sequence, no late Paleozoic zircons were recovered.

[61] Finally, a Jurassic to Lower Cretaceous sandstone was collected from the Xianza area (Figures 3 and 4). This sample yielded mainly >500 Ma zircons with a similar age distribution as the underlying strata, as well as zircons with ages of approximately 170 Ma, 235–285 Ma, 328 Ma, and 413 Ma (Table S4, Figure S4, and Figure 8). These ages are similar to those reported by *Leier et al.* [2007] from one Jurassic sample (LNPLA on Figure 8) and several Cretaceous samples collected from the eastern portion of the terrane.

[62] The provenance of detrital zircons in the Lhasa terrane appears to have changed upsection, much as in the Tethyan assemblage, with local granitic sources during early Paleozoic time giving way to broader Gondwana sources (characterized by a range of 500–1200 Ma detrital zircons) during Carboniferous through Cretaceous time (Figure 8). This is not surprising given that Lhasa is interpreted to have originated along the northern margin of India (and therefore adjacent to the Tethyan assemblage), prior to Triassic time [*Allégre et al.*, 1984; *Metcalfe*, 1996; *Yin and Nie*, 1996; *Yin and Harrison*, 2000] (Figures 13a–13e). The similarity of Lhasa and Tethyan detrital zircon ages does not support the view [*Zhu et al.*, 2010] that Lhasa was an isolated microcontinent within the Paleo-Tethys ocean basin during late Paleozoic time.

### 4.5. South Qiangtang Terrane

[63] Fourteen samples have been analyzed from the southern Qiangtang terrane, seven as part of this study (Table 1) and seven reported by *Pullen et al.* [2010]. The oldest samples include five from the Duguer Shan (Figure 3), which are intruded by ~475 Ma igneous rocks but contain zircons as young as 507–551 Ma (youngest cluster with n > 2). Primary age groups in these samples are 550–650 Ma, ~800 Ma, and ~950 Ma, with few grains that are >1.0 Ga (Figure S5, Table S5, and Figure 9).

[64] Five Carboniferous–Permian samples, most with diamictite texture, were also analyzed, and these samples yield very similar sets of 500–1000 Ma ages (Figure 9). Maximum depositional ages (youngest cluster with n > 2) for these samples are 537–559 Ma.

[65] The ages of zircons in Paleozoic strata strongly resemble the age distributions in strata of the Tethyan Sequence and Lhasa terrane (Figure 9). This is consistent with previous interpretations [e.g., *Yin and Nie*, 1996; *Metcalfe*, 1996] that Qiangtang was located in proximity to the Gondwana margin during late Paleozoic time (Figures 13a–13e).

[66] Four samples of Triassic sandstone yield very different age distributions, with significant 1.8–2.0 Ga and 200–300 Ma ages and few ages in the 500–1000 Ma range (Figure S5, Table S5, and Figure 9). Maximum depositional ages (youngest cluster with n > 2) are very similar to their depositional age, ranging from 215 to 235 Ma, which suggests that these grains were shed mainly from Triassic arc-type rocks present within the Qiangtang terrane [*Kapp et al.*, 2003; *Pullen et al.*, 2010]. The abundance of the Mesozoic grains presumably reflects the onset of Mesozoic arc-type magmatism within the Qiangtang terrane, whereas an influx of 1.8–2.0 Ga zircons may record arrival of the Qiangtang terrane in proximity to a northern realm with abundant 1.8–2.0 Ga crust (Figures 13f–13h).

### 4.6. North Qiangtang Terrane

[67] Our twelve samples from Carboniferous through Triassic strata (Figure S6 and Table S6) yield detrital zircon ages that are very similar to ages from samples of South Qiangtang. As shown on Figure 10, all seven of the older samples yield similar age distributions, with main age groups between 500 and 1000 Ma. Triassic samples reveal significantly different age distributions, with most ages between 240 and 330 Ma. The one Permian sample has an age distribution that is intermediate between older and younger samples, with main age ranges of 250–290 Ma, 440–500, and 740–1050 Ma.

[68] Maximum depositional ages (based on the peak age of n > 2 clusters) for the Carboniferous strata range from 516 to 571 Ma, which significantly pre-dates deposition. The maximum depositional ages for younger strata are closer to the depositional ages; 255 Ma for the Permian sample and 237–257 Ma for the Triassic samples.

[69] The high degree of similarity of the Carboniferous and Permian samples suggests that similar sources were contributing detritus to all of these units. To investigate the importance of sources that are represented by igneous cobbles in the sequence, zircons from eight granitic cobbles from one locality were analyzed separately. The interpreted

ages belong to two clusters, a younger group of clasts with interpreted weighted mean ages ranging from ca. 731 to 742 Ma, and an older group of clasts with interpreted ages of ca. 818 and 835 Ma (Table S7). When all analyses are plotted on an age distribution diagram, peak ages are at 737 and 820 Ma (Figure 10). The lack of overlap between the distribution of ages in cobbles and the sandstone matrix is striking. This difference presumably reflects derivation of the cobbles from this particular horizon from a restricted source region and transport as glacial dropstones, versus derivation of most sandstone matrix from a broad source region in a well-mixed sedimentary system.

[70] As with South Qiangtang, the Triassic strata reveal detrital zircon ages that are significantly different from underlying Carboniferous–Permian diamictite (Figures 13d–13f), suggesting derivation from a different source region and little recycling of the older strata. An interesting difference from South Qiangtang, however, is that zircons in North Qiangtang tend to be older (peak ages of 251–268) than in South Qiangtang (peak ages of 217–235 Ma). This suggests that the proportions of Permian versus Triassic magmatism may have been different in the two portions of the Qiangtang terrane.

[71] The provenance of North Qiangtang Permian strata is less well constrained given that only one sample was analyzed. A reasonable explanation, however, is that the Permian strata received detritus from the same sources as the underlying diamictites, or were recycled from the diamictites, and also received considerable first-cycle detritus from nearby igneous activity.

[72] The similarity of age distributions from the northern and southern portions of the Qiangtang terrane is consistent with previous models [*Kapp et al.*, 2003; *Pullen et al.*, 2010] in which the two regions belong to a single crustal fragment. Our data are less supportive of suggestions that north and south Qiangtang terranes belong to two distinct crustal fragments [*Li*, 1987; *Kidd et al.*, 1988; *Metcalfe*, 1988, 1996; *Şengör et al.*, 1988; *Li et al.*, 1995; *Zhang*, 2001].

### 4.7. Songpan Ganzi Complex

[73] Detrital zircon ages from the Songpan Ganzi complex have previously been reported by *Bruguier et al.* [1997], *Weislogel et al.* [2006, 2010], and *Wang et al.* [2009]. Sampled strata are mainly Middle–Late Triassic in age, and were collected from a broad region of the eastern portion of the terrane (Figure 1). Primary age groups are 212–537 Ma with age peaks at ~263 and 440 Ma, 720–850 Ma with age peaks at 770 and 793 Ma, 1730–2100 Ma with an age peak at 1870 Ma, and 2360–2630 Ma with an age peak at 2515 Ma (Figure 11).

[74] There has been considerable debate about the provenance of the thick succession of marine clastic strata in the Songpan Ganzi complex [*Yin and Nie*, 1993; *Nie et al.*, 1994; *Zhou and Graham*, 1996]. The Sognpan–Ganzi complex contains abundant middle to late Paleozoic zircons and conspicuously lacks significant 900–1200 Ma zircons common in terranes to the south/southwest (Figure 11). Therefore, most workers agree that much of the Songpan Ganzi detritus originated from the Qinling–Dabie orogen, which separates the North China and South China cratons, as well as the Kunlun orogen, North China craton, and

South China craton [*Zhou and Graham*, 1996; *Bruguier et al.*, 1997; *Weislogel et al.*, 2006, 2010; *Enkelmann et al.*, 2007] (Figures 1 and 13g). The large volume of detritus in the eastern Songpan Ganzi basin was apparently generated from erosion of Paleozoic synorogenic continental and island arc magmatic igneous rocks and related sedimentary rocks of this compound orogen system during final Triassic collision. However, provenance of the central and western Songpan–Ganzi remains unstudied and could have had other origins. The Songpan–Ganzi basin subsequently collapsed and inverted during Jurassic accretion of the Qiangtang terrane and formation of the Jinsa suture [*Zhou and Graham*, 1996; *Yin and Nie*, 1996; *Yin and Harrison*, 2000; *Weislogel et al.*, 2006, 2010; *Wang et al.*, 2009] (Figures 13g and 13h).

### 4.8.  Qilian Shan–Nan Shan–Altun Shan Terrane(s)

[75]  *Gehrels and Yin* [2003a] analyzed detrital zircons from eight samples collected from the Qilian Shan, Nan Shan, and Altun Shan terranes. These samples have been reanalyzed by LA–ICPMS (~100 grains each) for more complete provenance constraints, and are reported herein (Table S7 and Figure S7). The reanalyzed samples include two from metasedimentary assemblages that are intruded by early Paleozoic plutons, and therefore assumed to be of Proterozoic age, four samples that are interpreted to be part of the early Paleozoic arc system (most likely Ordovician in age), and overlying Silurian (?) and Jurassic sandstones.

[76]  The two Proterozoic (?) samples yield very different age spectra, with an ultramature quartzite from the Altun Shan containing mainly 1.2–2.0 Ga and 2.4–2.8 Ga grains, and quartz-rich metaturbidite sequence from the Nan Shan containing mainly ~800 Ma grains and subordinate >1.8 Ga grains (Figure 11). The ~800 Ma grains were presumably derived from a metaplutonic and metavolcanic arc (?) assemblage that forms the basement to the early Paleozoic arc system (Figures 13a).

[77]  Ordovician strata are volcanic-rich sandstones that include predominantly 450–490 Ma detrital zircons interpreted to have been derived from local magmatic arcs (Figures 11 and 13b). One sample contains a few of these grains but is dominated by ~920 Ma grains, which is also a common age for the underlying Proterozoic meta-igneous basement. Overlying Silurian (?) strata include both ~800 Ma and ~450 Ma zircons derived from underlying igneous systems (Figure 13c), whereas Jurassic strata include some early Paleozoic zircons but are dominated by zircons of 270–280 Ma. The latter grains were presumably shed from the Kunlun terrane, which contains widespread igneous rocks of this age [*Harris et al.*, 1988a; *Xiao et al.*, 2002] (Figure 13g). The 400–520 Ma zircons are interpreted to have been shed from local plutonic rocks that yield similar ages [*Gehrels and Yin*, 2003b]. A probability plot of these ages is shown on Figure 11.

### 4.9.  Tarim Terrane

[78]  Our detrital zircon samples were collected from Proterozoic (?) sandstone units that rest directly on the older basement complexes. These strata were originally analyzed by *Gehrels and Yin* [2003b]: additional analyses are reported herein (Table S8 and Figure S7). Ages from these samples are mainly 1.8–2.1 Ga (peak ages of 1888 and 1946 Ma;

Figure 11), which matches the Paleoproterozoic age of igneous rocks of the southern Tarim craton [*Gehrels and Yin*, 2003b].

## 5.  Tectonic Synthesis

[79]  The detrital zircon age distributions described above provide new information that can be used to aid in reconstructing the pre-Cenozoic tectonic evolution of the Tibetan–Himalayan orogen. There are challenges in using this data for tectonic analysis, however, as follows:

[80]  1. Cratons surrounding the Tibet–Himalayan orogen tend to have similar ages of Late Archean and Early Proterozoic igneous activity (e.g., Figure 12), which makes it difficult to distinguish unique sources for the older zircons present in most samples.

[81]  2. Much of Gondwana experienced magmatism between 500 and 1200 Ma, as summarized recently by *Myrow et al.* [2010], which prevents identification of specific sources for the dominant grains in much of the orogen.

[82]  3. Early Paleozoic igneous activity within the orogen overlaps in age with Gondwana-wide igneous activity, making it difficult to distinguish local versus distant sources for early Paleozoic zircons.

[83]  4. During late Paleozoic time, glaciogenic sediment appears to have blanketed a large region surrounding Gondwana, which ties these assemblages to the southern hemisphere but prevents more detailed paleogeographic analysis.

[84]  5. The presence of coeval late Paleozoic–Mesozoic magmatic arcs in several terranes makes it difficult to tie zircons of these ages to specific igneous sources.

[85]  In spite of these challenges, detrital zircon ages provide an independent means of evaluating conclusions based on geologic, paleomagnetic, and biogeographic data, as summarized by *Dewey et al.* [1988], *Hsü et al.* [1995], *Şengör and Natal'in* [1996a], *Metcalfe* [1996], *Yin and Nie* [1996], *Yin and Harrison* [2000], *Heubeck* [2001], *Blakey* [2008], and *Ferrari et al.* [2008]. Following is a chronological discussion of the provenance interpretations and their tectonic implications (Figures 13 and 14), referenced to age-distribution plots appropriate for Proterozoic through early Paleozoic time (Figure 12a), late Paleozoic time (Figure 12b), and Mesozoic time (Figure 12c).

### 5.1.  Proterozoic Through Early Paleozoic Time

[86]  Detrital zircons in Upper Proterozoic and lower Paleozoic strata throughout Tibet and the Himalaya are mainly <1.4 Ga, with most grains between 500 and 1200 Ma (Figure 12a). These zircons are interpreted to have been shed primarily from convergent margin systems that are preserved within the East African orogen and the Ross–Delamerian orogen of Gondwana [*DeCelles et al.*, 2000; *Myrow et al.*, 2010] (Figures 13a and 13b). During early Paleozoic time it appears that three convergent margin systems were present:

[87]  1. A north-facing system along the northern margin of India that generated the Cambro–Ordovician granites of the Himalaya [e.g., *LeFort*, 1975, 1996; *LeFort et al.*, 1986; *Cawood et al.*, 2007], and is associated with regional metamorphism (to garnet grade) [*Marquer et al.*, 2000; *Gehrels et al.*, 2006a, 2006b, 2008; *Cawood et al.*, 2007;

*Martin et al.*, 2007] and regional uplift and erosion [*Hayden*, 1904; *Garzanti et al.*, 1986; *Gaetani and Garzanti*, 1991; *Brookfield*, 1993; *Garzanti*, 1999; *Myrow et al.*, 2006b; *Johnson et al.*, 2001]. This system is interpreted to have extended across the northern margin of India, forming a proto-Himalayan orogen [*LeFort et al.*, 1986, *Garzanti et al.*, 1986; *Brookfield*, 1993; *Gehrels et al.*, 2003; *Cawood et al.*, 2007; *Myrow et al.*, 2006a, 2006b; *Johnson et al.*, 2001]. Cambro–Ordovician granitic rocks of the Lhasa, Amdo [*Guynn et al.*, 2006, 2011], and Qiangtang terranes [*Pullen et al.*, 2010] are interpreted to have formed within this convergent margin system. As described by *Cawood and Buchan* [2007] and *Cawood et al.* [2007], similar convergent/orogenic systems extended around much of the Gondwana margin during early Paleozoic time (Figures 13a and 13b). As an alternative view, *Miller et al.* [2001] argue that this early Paleozoic orogen is extensional in origin on the basis of the geochemistry of Himalayan granitoids.

[88] 2. A south-facing system in the Kunlun orogen, which is interpreted to have been built along the southern margin of the amalgamated Nan Shan–Qilian Shan–Altun Shan–Qaidam–Kunlun terrane [*Dewey et al.*, 1988; *Hsü et al.*, 1995; *Yin and Nie*, 1996; *Şengör and Natal'in*, 1996a; *Yin and Harrison*, 2000].

[89] 3. A north-facing arc that is interpreted to have brought the Nan Shan–Qilian Shan–Altun Shan terrane into juxtaposition with the southern margin of the Tarim craton during Ordovician–Silurian time [*Yin and Nie*, 1996; *Sobel and Arnaud*, 1999; *Gehrels and Yin*, 2003a, 2003b] (Figures 13a–13c).

[90] Convergent-margin magmatism appears to have ceased throughout the Tibetan–Himalayan realm following Ordovician–Silurian time, as Devonian–Carboniferous igneous rocks and detrital zircons are rare (Figures 12a and 12b). One possible explanation for this lack of magmatism is that Ordovician–Silurian convergence closed all of the separating (pre-Tethyan or proto-Tethyan) ocean basins such that Lhasa, Qiangtang, and Nan Shan–Qilian Shan–Altun Shan terranes were caught between the Tarim and Indian cratons in much their present configuration (Figures 13b and 13c). Break-up of this proto-Tibetan orogen appears to have occurred during Devonian time [*Metcalfe*, 1996] with formation of the Paleo-Tethys ocean basin between the Nan Shan–Qilian Shan–Altun Shan terrane and the Qiangtang terrane.

## 5.2. Late Paleozoic Time

[91] Upper Paleozoic strata of the upper Lesser Himalaya, Tethyan Sequence, Lhasa terrane, and both north and south Qiangtang consist of a very similar suite of ages (Figure 12b), with main age groups of 450–550 Ma, ~620 Ma, ~800 Ma, and ~970 Ma. Because most of these strata are diamictites, and ice-rafted debris can travel vast distances, it is likely that the ultimate source of the detritus was within the polar ice cap that covered most of Antarctica, southern Australia, and India [*Dewey et al.*, 1988; *Metcalfe*, 1996; *Blakey*, 2008] (Figure 13c). The presence of the diamictite and its diagnostic detrital zircon age distribution indicates that the northern Qiangtang terrane is not of Laurasian affinity, as has been argued by *Li et al.* [1995], *Metcalfe* [1996], *Bao et al.* [1999], and *Zhang* [2001]. Permian magmatism recorded within Mesozoic strata of the upper

Lesser Himalaya, Tethyan Sequence, Lhasa terrane, and Qiangtang terrane may reflect rifting events that separated Qiangtang and Lhasa from each other and from the northern Indian margin [*Gaetani and Garzanti*, 1991; *Brookfield*, 1993; *Yin and Nie*, 1996; *Metcalfe*, 1996; *Garzanti*, 1999; *Yin and Harrison*, 2000], although *Baxter et al.* [2009] argue that Qiangtang–Lhasa separation did not occur until Late Triassic or even Jurassic time (Figures 13d–13f). It is also possible that a small ocean basin opened and then closed within the Lhasa terrane during Permian time [*Zhu et al.*, 2009, 2010].

## 5.3. Mesozoic Time

[92] During Mesozoic (and latest Paleozoic) time there was a major shift in provenance within the northern terranes due to the onset of Permo–Triassic arc-type magmatism (Figure 12c). The proportion of this young magmatism increases northward, with a few 235–285 Ma and ~170 Ma grains in the Lhasa terrane, a significant percentage of 194–291 Ma grains (age peaks at 234, 254, and 281 Ma) in the south Qiangtang terrane, and mostly 220–300 Ma grains (age peak at 256 Ma) in the north Qiangtang terrane. These magmatic arcs also supplied sediment to the Songpan–Ganzi complex, particularly its western parts [*Bruguier et al.*, 1997; *Weislogel et al.*, 2006, 2010; *She et al.*, 2006; *Weislogel*, 2008; *Wang et al.*, 2009]. As described recently by *Pullen et al.* [2008], this magmatism may have resulted from south-facing subduction beneath the Kunlun terrane (on the southern margin of the Nan Shan–Qilian Shan–Altun Shan–Qaidam–Kunlun margin), north-facing subduction beneath the Qiangtang terrane, and south-facing subduction along the southern margin of the Qiangtang terrane (Figures 13e–13h and Figure 14).

[93] Qiangtang Triassic strata also show possible connections with the Tarim craton and Nan Shan–Qilian Shan–Altun Shan terrane through the presence of Ordovician–Silurian (age peaks of 445 Ma in South Qiangtang, 445 Ma in North Qiangtang, 440 Ma in Songpan Ganzi, and 432 in Nan Shan–Qilian Shan–Altun Shan) and 1.8–2.0 Ga grains (Figure 12c). This contrasts with their provenance during late Paleozoic time, which appears to have been dominated by Gondwana.

[94] Young magmatism was also significant along the northern Indian margin, as recorded by the abundance of 120–130 Ma zircons in Cretaceous strata of the Himalaya. As suggested by *Gaetani and Garzanti* [1991], *Brookfield* [1993], *Garzanti* [1999], *DeCelles et al.* [2000], and *Hu et al.* [2008, 2009], this magmatism may have resulted from extension as India rifted from Gondwana and began its northward migration toward Asia (Figure 13h).

## 6. Conclusions

[95] This compilation provides an opportunity for the first regional synthesis of detrital zircon data from the Tibet–Himalayan region. In spite of the non-uniqueness of some of the data, and a lack of data from some regions (e.g., Kunlun and Qaidam regions) and time periods (e.g., Devonian), several first-order conclusions are offered:

[96] 1. Most strata in crustal fragments that make up Tibet and the Himalaya are dominated by detrital zircon ages that are younger than 1.4 Ga. The scarcity of Paleoproterozoic

and Archean zircons suggests that these strata accumulated with little influence from surrounding cratons and that little pre-mid-Proterozoic crust is present within these fragments. Although U-Pb ages are not a direct record of crustal genesis, this observation is consistent with the hypothesis that much of the Tibet–Himalayan orogen consists of relatively juvenile crust [*Dewey et al.*, 1988].

[97]  2. Growth of crust in the Tibet–Himalayan region appears to have occurred largely during Neoproterozoic and early Paleozoic time through the formation of magmatic arcs, accretionary complexes, and marginal ocean basins (Figures 13a–13c, 14a, and 14b). Formation of crust in this type of convergent margin setting is consistent with previously proposed archipelago [*Hsü et al.*, 1995], Turkic-style [*Şengör and Natal'in*, 1996a, 1996b], and accretionary [*Cawood and Buchan*, 2007] models for crustal genesis.

[98]  3. The earliest phase of igneous activity in the Tibet–Himalaya region is recorded by ~900–600 Ma igneous rocks preserved within the Nan Shan–Qilian Shan–Altun Shan terrane [*Gehrels and Yin*, 2003b] and in Amdo basement [*Guynn et al.*, 2006, 2011]. These rocks are interpreted to be restricted exposures of arc-type basement that may be widespread within the Tibet–Himalaya region, and may represent a northeasterly continuation of juvenile terranes in the Arabian–Nubian Shield [*Stern*, 1994; *Johnson and Woldehaimanot*, 2003] (Figure 13a).

[99]  4. The second main phase of igneous activity is recorded by early Paleozoic arc-type igneous rocks within the Greater Himalayan sequence, Lhasa terrane, Amdo basement, and Qiangtang terrane, which are interpreted to record convergent-margin magmatism and tectonism along the northern margin of Gondwana during early Paleozoic time (Figures 13a, 13b, 14a, and 14b). This style of tectonism is found around most other portions of Gondwana during early Paleozoic time [e.g., *Cawood and Buchan*, 2007; *Cawood et al.*, 2007].

[100]  5. Glaciogenic sediment derived from a polar ice cap centered on Antarctica, southern Australia, and southern India are present in all terranes south of the Jinsa suture, which suggests that these fragments were in proximity to Gondwana through Carboniferous–Permian time (Figures 13d and 13e). Such broad dispersal of this marine sediment may reflect the lack of emergent orogenic highlands and magmatic arcs in the Tibetan region during mid-Paleozoic time.

[101]  6. The Nan Shan–Qilian Shan–Altun Shan terrane in northern Tibet records a very different history from more southern crustal fragments during Paleozoic time in terms of faunal affinities (as summarized by *Metcalfe* [1996]), geologic/tectonic history [*Dewey et al.*, 1988; *Hsü et al.*, 1995; *Şengör and Natal'in*, 1996a; *Yin and Nie*, 1996; *Yin and Harrison*, 2000; *Heubeck*, 2001; *Blakey*, 2008; *Ferrari et al.*, 2008], and detrital zircon ages (Figure 12). This terrane instead appears to have formed and resided in proximity to the Tarim–North China craton to the north (Figures 13a, 13b, 14a, and 14b).

[102]  7. The fundamental boundary between terranes of Gondwana affinity (Cimmerian terranes of *Stampfli and Borel* [2002] and *Blakey* [2008]) and Laurasian affinity (Hunic terranes, *op. cit.*) is presently located along the Jinsa suture (Figure 1). Although the present juxtaposition of rocks from these two domains results from closure of the Songpan–Ganzi basin during Jurassic time, they may have previously been juxtaposed during mid-Paleozoic time [*Kapp et al.*, 2003] (Figures 13 and 14) A cryptic deformational event described in the Kunlun Shan [*Dewey et al.*, 1988] may record this Silurian–Devonian (?) collisional event.

[103]  8. The detrital zircon record of the Qiangtang and Lhasa terranes changes dramatically during Triassic time, with most sediment derived from intraterrane magmatic arcs and also from the Nan Shan–Qilian Shan–Altun Shan terranes to the north. This timing is consistent with previous interpretations that the Meso-Tethys (between Qiangtang and Lhasa) and Neo-Tethys (between Lhasa and the northern Indian margin) were open by Triassic time [*Dewey et al.*, 1988; *Yin and Nie*, 1996; *Metcalfe*, 1996; *Yin and Harrison*, 2000; *Blakey*, 2008] (Figures 13 and 14).

[104]  9. Our data support a four-stage history [e.g., *Dewey et al.*, 1988; *Metcalfe*, 1996] of the origin and displacement of crustal fragments in the Tibet–Himalayan orogen: formation along the Gondwana margin during early Paleozoic time, rifting and northward displacement across Tethyan ocean basins (at least three) during late Paleozoic through Jurassic time, progressive accretion to the southern margin of Asia starting in Jurassic time, and final consolidation with the arrival of India during latest Cretaceous–early Tertiary time (Figures 13 and 14).

[105]  It is important to note that this synthesis is built on a sizable data set, but that there are still large and significant gaps in the available information. For example, we have no detrital zircon constraints from pre-Mesozoic strata in the Kunlun Shan and Qaidam basin. For the purposes of this study these regions are interpreted to have experienced the same post–Ordovician history as the Nan Shan–Qilian Shan–Altun Shan, but this clearly needs to be tested. In addition, there are significant gaps in the stratigraphic coverage from each region (Figure 12). This is unfortunate given the need to compare detrital zircon ages from age-equivalent strata. Clearly this study is preliminary in nature, and conclusions based on detrital zircon data will be refined as additional data become available.

## References

Ali, J., and J. Aitchison (2008), Gondwana to Asia: Plate tectonics, paleogeography, and the biological connectivity of the Indian subcontinent from the Middle Jurassic through latest Eocene (166–35 Ma), *Earth Sci. Rev.*, *88*, 145–166, doi:10.1016/j.earscirev.2008.01.007.

Allégre, C. J., et al. (1984), Structure and evolution of the Himalayan–Tibet orogenic belt, *Nature*, *307*, 17–22, doi:10.1038/307017a0.

Andersen, T. (2005), Detrital zircons as tracers of sedimentary provenance: Limiting conditions from statistics and numerical simulation, *Chem. Geol.*, *216*(3–4), 249–270, doi:10.1016/j.chemgeo.2004.11.013.

Bao, P. S., X. C. Xiao, J. Wang, C. Li, and K. Hu (1999), The blueschist belt in the Shuanghu region, central–northern Tibet, and its tectonic implications, *Dizhi Xuebao*, *72*, 304–312.

Baxter, A. T., J. C. Aitchison, and S. V. Zyabrev (2009), Radiolarian age constraints on Mesotethyan ocean evolution, and their implications for development of the Bangong–Nujiang suture, *J. Geol. Soc.*, *166*, 689–694, doi:10.1144/0016-76492008-128.

Blakey, R. C. (2008), Gondwana paleogeography from assembly to breakup—A 500 m.y. odyssey, in *Resolving the Late Paleozoic Ice Age in Time and Space*, edited by C. R. Fielding, T. D. Frank, and J. L. Isbell, *Spec. Pap. Geol. Soc. Am.*, *441*, 1–28.

Bordet, P., M. Colchen, D. Krummenacher, P. LeFort, R. Mouterde, and M. Remy (1971), *Recherches Geologiques dans l'Himalaya du Nepal, Region de la Thakkhola*, 279 pp., Cent. Natl. de la Rech. Sci., Paris.

Brookfield, M. E. (1993), The Himalayan passive margin from Precambrian to Cretaceous times, *Sediment. Geol.*, *84*, 1–35, doi:10.1016/0037-0738(93)90042-4.

Bruguier, O., J. R. Lancelot, and J. Malavielle (1997), U-Pb dating on single detrital zircon grains from the Ttiassic Songpan–Ganzi flysch (Central China): Provenance and tectonic correlations, *Earth Planet. Sci. Lett.*, *152*, 217–231, doi:10.1016/S0012-821X(97)00138-6.

Burg, J. P., and G. M. Chen (1984), Tectonics and zonation of southern Tibet, China, *Nature*, *311*, 219–223, doi:10.1038/311219a0.

Cawood, P. A., and C. Buchan (2007), Linking accretionary orogenesis with supercontinent assembly, *Earth Sci. Rev.*, *82*, 217–256, doi:10.1016/j.earscirev.2007.03.003.

Cawood, P. A., M. R. W. Johnson, and A. A. Nemchin (2007), Early Paleozoic orogenesis along the Indian margin of Gondwana: Tectonic response to Gondwana assembly, *Earth Planet. Sci. Lett.*, *255*, 70–84, doi:10.1016/j.epsl.2006.12.006.

Célérier, J., T. M. Harrison, A. A. G. Webb, and A. Yin (2009), The Kumaun and Garwhal Lesser Himalaya, India: Part 1. Structure and stratigraphy, *Geol. Soc. Am. Bull.*, *121*, 1262–1280, doi:10.1130/B26344.1.

Chang, C., and X. Zheng (1973), Some tectonic features of the Mt. Jomo Lungma area, southern Tibet, *Sci. Sin.*, *16*, 257–265.

Colchen, M., P. LeFort, and A. Pêcher (1986), *Annapurna, Manaslu, Ganesh Himal*, 136 pp., Cent. Natl. de la Rech. Sci., Paris.

Coward, M. P., W. S. F. Kidd, Y. Pan, R. M. Shackleton, and H. Zhang (1988), The structure of the 1985 Tibet Geotraverse: Lhasa to Golmud, *Philos. Trans. R. Soc. London, Ser. A*, *327*, 307–333, doi:10.1098/rsta.1988.0131.

Darby, B. J., and G. E. Gehrels (2006), Detrital zircon reference for the North China block, *J. Asian Earth Sci.*, *26*, 637–648, doi:10.1016/j.jseaes.2004.12.005.

DeCelles, P. G., G. E. Gehrels, J. Quade, B. Lareau, and M. Spurlin (2000), Tectonic implications of U-Pb zircon ages of the Himalayan orogenic belt in Nepal, *Science*, *288*, 497–499, doi:10.1126/science.288.5465.497.

DeCelles, P. G., D. M. Robinson, J. Quade, T. P. Ojha, C. N. Garzione, P. Copeland, and B. N. Upreti (2001), Stratigraphy, structure, and tectonic evolution of the Himalayan fold–thrust belt in western Nepal, *Tectonics*, *20*, 487–509, doi:10.1029/2000TC001226.

DeCelles, P. G., G. E. Gehrels, Y. Najman, A. J. Martin, A. Carter, and E. Garzanti (2004), Detrital geochronology and geochemistry of Cretaceous–Early Miocene strata of Nepal: Implications for timing and diachroneity of initial Himalayan orogenesis, *Earth Planet. Sci. Lett.*, *227*, 313–330, doi:10.1016/j.epsl.2004.08.019.

Dewey, J. F., and K. Burke (1973), Tibetan, Variscan, and Precambrian basement reactivation: Products of continental collision, *J. Geol.*, *81*, 683–692, doi:10.1086/627920.

Dewey, J. F., R. M. Shackelton, C. Chengfa, and S. Yiyin (1988), The tectonic evolution of the Tibetan Plateau, *Philos. Trans. R. Soc. London, Ser. A*, *327*, 379–413, doi:10.1098/rsta.1988.0135.

Dickinson, W. R., and G. E. Gehrels (2009), Use of U-Pb ages of detrital zircons to infer maximum depositional ages of strata: A test against a Colorado Plateau Mesozoic database, *Earth Planet. Sci. Lett.*, *288*, 115–125, doi:10.1016/j.epsl.2009.09.013.

Ding, L., P. Kapp, D. Zhong, and W. Deng (2003), Cenozoic volcanism in Tibet: Evidence for a transition from oceanic to continental subduction, *J. Petrol.*, *44*, 1833–1865, doi:10.1093/petrology/egg061.

Dürr, S. B. (1996), Provenance of Xigaze fore-arc basin clastic rocks (Cretaceous, south Tibet), *Geol. Soc. Am. Bull.*, *108*(6), 669–684, doi:10.1130/0016-7606(1996)108<0669:POXFAB>2.3.CO;2.

Dürr, S. B., and M. R. Gibling (1994), Early Cretaceous volcaniclastic and quartzose sandstones from north-central Nepal: Composition, sedimentology, and geotectonic significance, *Geol. Rundsch.*, *83*, 62–75, doi:10.1007/BF00211894.

Enkelmann, E., A. Weislogel, L. Ratschbacher, E. Eide, A. Renno, and J. Wooden (2007), How was the Triassic Songpan–Ganzi basin filled? A provenance study, *Tectonics*, *26*, TC4007, doi:10.1029/2006TC002078.

Fedo, C. M., K. Sircombe, and R. Rainbird (2003), Detrital zircon analysis of the sedimentary record, in *Zircon, Rev. Mineral. Geochem.*, vol. 53, edited by J. M. Hanchar and P. W. O. Hoskin, pp. 277–303, Mineral. Soc. of Am., Washington, D. C.

Ferrari, O. M., C. Hochard, and G. M. Stampfli (2008), An alternative plate tectonic model for the Palaeozoic–Early Mesozoic Palaeotethyan evolution of Southeast Asia (Northern Thailand–Burma), *Tectonophysics*, *451*, 346–365, doi:10.1016/j.tecto.2007.11.065.

Fuchs, G., R. Widder, and R. Tuladhar (1988), Contributions to the geology of the Annapurna Range (Manang area, Nepal), *Jahrb. Geol. Bundesanst.*, *131*, 593–607.

Gaetani, M., and E. Garzanti (1991), Multicyclic history of the northern India continental margin (northwestern Himalaya), *AAPG Bull.*, *75*(9), 1427–1446.

Gansser, A. (1964), *Geology of the Himalayas*, 289 pp., Wiley Intersci., London.

Garzanti, E. (1999), Stratigraphy and sedimentary history of the Nepal Tethys Himalaya passive margin, *J. Asian Earth Sci.*, *17*, 805–827, doi:10.1016/S1367-9120(99)00017-6.

Garzanti, E. (2008), Comment on "When and where did India and Asia collide?" by Jonathan C. Aitchison, Jason R. Ali, and Aileen M. Davis, *J. Geophys. Res.*, *113*, B04411, doi:10.1029/2007JB005276.

Garzanti, E., R. Casnedi, and F. Jadoul (1986), Sedimentary evidence of a Cambro–Ordovician orogenic event in the northwestern Himalaya, *Sediment. Geol.*, *48*, 237–265, doi:10.1016/0037-0738(86)90032-1.

Gehrels, G. E. (2000), Introduction to detrital zircon studies of Paleozoic and Triassic strata in western Nevada and northern California, in *Paleozoic and Triassic Paleogeography and Tectonics of Western Nevada and Northern California*, edited by M. J. Soreghan and G. E. Gehrels, *Spec. Pap. Geol. Soc. Am.*, *347*, 1–18.

Gehrels, G. E. (2011), Detrital zircon U-Pb geochronology: Current methods and new opportunities, in *Recent Advances in Tectonics of Sedimentary Basins*, edited by C. Busby and A. Azor, Wiley-Blackwell, Hoboken, N. J., in press.

Gehrels, G. E., and A. Yin (2003a), Detrital zircon geochronology of the northeastern Tibetan Plateau, *Geol. Soc. Am. Bull.*, *115*, 881–896, doi:10.1130/0016-7606(2003)115<0881:DGOTNT>2.0.CO;2.

Gehrels, G. E., and A. Yin (2003b), Magmatic history of the northeastern Tibetan Plateau, *J. Geophys. Res.*, *108*(B9), 2423, doi:10.1029/2002JB001876.

Gehrels, G. E., P. G. DeCelles, A. Martin, T. P. Ojha, G. Pinhassi, and B. N. Upreti (2003), Initiation of the Himalayan orogen as an early Paleozoic thin-skinned thrust belt, *GSA Today*, *13*(9), 4–9, doi:10.1130/1052-5173(2003)13<4:IOTHOA>2.0.CO;2.

Gehrels, G. E., P. G. DeCelles, T. P. Ojha, and B. N. Upreti (2006a), Geologic and U-Th-Pb geochronologic evidence for early Paleozoic tectonism in the Kathmandu thrust sheet, central Nepal Himalaya, *Geol. Soc. Am. Bull.*, *118*, 185–198, doi:10.1130/B25753.1.

Gehrels, G. E., P. G. DeCelles, T. P. Ojha, and B. N. Upreti (2006b), Geologic and U-Pb geochronologic evidence for early Paleozoic tectonism in the Dadeldhura thrust sheet, far-west Nepal Himalaya, *J. Asian Earth Sci.*, *28*, 385–408, doi:10.1016/j.jseaes.2005.09.012.

Gehrels, G. E., V. Valencia, and A. Pullen (2006c), Detrital zircon geochronology by Laser–Ablation Multicollector ICPMS at the Arizona LaserChron Center, in *Geochronology: Emerging Opportunities, Paleontological Society Short Course, October 21, 2006, Philadelphia, PA*, edited by T. Olszewski and W. Huff, *Paleontol. Soc. Pap.*, *12*, 1–10.

Gehrels, G. E., V. Valencia, and J. Ruiz (2008), Enhanced precision, accuracy, efficiency, and spatial resolution of U-Pb ages by laser ablation–multicollector–inductively coupled plasma–mass spectrometry, *Geochem. Geophys. Geosyst.*, *9*, Q03017, doi:10.1029/2007GC001805.

Goodwin, A. M. (1996), *Principles of Precambrian Geology*, 327 pp., Academic, San Diego, Calif.

Guynn, J., P. Kapp, A. Pullen, M. Heizler, G. Gehrels, and L. Ding (2006), Tibetan basement rocks near Amdo reveal "missing" Mesozoic tectonism along the Bangong suture, central Tibet, *Geology*, *34*, 505–508, doi:10.1130/G22453.1.

Guynn, J., P. Kapp, G. Gehrels, and L. Ding (2011), U-Pb geochronology of basement rocks in central Tibet and paleogeographic implications, *J. Asian Earth Sci.*, in press.

Harris, N. B. W., R. Xu, C. L. Lewis, C. J. Hawkesworth, and Y. Zhang (1988a), Isotope geochemistry of the 1985 Tibet Geotraverse, Lhasa to Glomud, *Philos. Trans. R. Soc. London, Ser. A*, *327*, 263–285, doi:10.1098/rsta.1988.0129.

Harris, N. B. W., T. J. B. Holland, and A. G. Tindle (1988b), Metamorphic Rocks of the 1985 Tibet Geotraverse, Lhasa to Golmud, *Philos. Trans. R. Soc. A*, *327*(1594), 203–213, doi:10.1098/rsta.1988.0126.

Hayden, H. H. (1904), The geology of Spiti with parts of Bahahr and Rupshu, *Mem. Geol. Surv. India*, *36*(1), 129 pp.

Heim, A., and A. Gansser (1939), Central Himalaya: Geological observations of the Swiss expedition 1936, *Denkschr. Schweiz. Naturforsch. Ges.*, *73*, 1–246.

Hennig, A. (1915), Zur Petrographie und Geologie von Sudwest Tibet, in *Southern Tibet*, vol. 5, edited by S. Hedin, Norstedt, Stockholm.

Heubeck, C. (2001), Assembly of central Asia during the middle and late Paleozoic, in *Paleozoic and Mesozoic Tectonic Evolution of Central Asia: From Continental Assembly to Intracontinental Deformation*, edited by M. S. Hendrix and G. A. Davis, *Mem. Geol. Soc. Am.*, *194*, 1–22.

Hodges, K. V. (2000), Tectonics of the Himalaya and southern Tibet from two perspectives, *Geol. Soc. Am. Bull.*, *112*, 324–350, doi:10.1130/0016-7606(2000)112<324:TOTHAS>2.0.CO;2.

Hsü, K. J., P. Guitang, and A. M. C. Şengör (1995), Tectonic evolution of the Tibetan Plateau: A working hypothesys based on the Archipelago model of orogenesis, *Int. Geol. Rev.*, *17*, 474–508.

Hu, X., L. Jansa, and C. Wang (2008), Upper Jurassic–Lower Cretaceous stratigraphy in south-eastern Tibet: A comparison with the western Himalayas, *Cretaceous Res.*, *29*, 301–315, doi:10.1016/j.cretres.2007.05.005.

Hu, X., L. Jansa, L. Chen, W. L. Griffin, S. Y. O'Reilly, and J. Wang (2009), Provenance of Lower Cretaceous Wolong volcaniclastics in the Tibetan Himalaya, Implications for the final breakup of eastern Gondwana, *Sediment. Geol.*, *223*(3–4), 193–205.

Hughes, N. C., S. Peng, O. N. Bhargava, A. D. Ahluwalla, P. M. Myrow, and S. K. Parcha (2005), Cambrian biostratigraphy of the Tal Group, Lesser Himalaya, India, and early Tsanglangpuan (late early Cambrian) trilobites from the Nigali Dhar syncline, *Geol. Mag.*, *142*(1), 57–80, doi:10.1017/S0016756804000366.

Johnson, P. R., and B. Woldehaimanot (2003), Development of the Arabian–Nubian Shield: Perspectives on accretion and deformation in the northern East African Orogen and the assembly of Gondwana, in *Proterozoic East Gondwana: Supercontinent Assembly and Breakup*, *Geol. Soc. Spec. Publ.*, *206*, 289–325.

Johnson, M. R. W., G. J. H. Oliver, R. R. Parrish, and S. P. Johnson (2001), Synthrusting metamorphism, cooling, and erosion of the Himalayan Kathmandu complex, Nepal, *Tectonics*, *20*, 394–415, doi:10.1029/2001TC900005.

Kapp, P., A. Yin, C. E. Manning, M. Murphy, T. M. Harrison, M. Spurlin, L. Ding, X.-G. Deng, and C. M. Wu (2000), Blueschist-bearing metamorphic core complexes in the Qiangtang block reveal deep crustal structure of northern Tibet, *Geology*, *28*, 19–22, doi:10.1130/0091-7613(2000)28<19:BMCCIT>2.0.CO;2.

Kapp, P., A. Yin, C. E. Manning, T. M. Harrison, M. H. Taylor, and D. Lin (2003), Tectonic evolution of the early Mesozoic blueschist-bearing Qiangtang metamorphic belt, central Tibet, *Tectonics*, *22*(4), 1043, doi:10.1029/2002TC001383.

Kapp, P., P. G. DeCelles, G. E. Gehrels, M. Heizler, and L. Ding (2007), Geological records of the Cretaceous Lhasa–Qiangtang and Indo–Asian collisions in the Nima basin area, central Tibet, *Geol. Soc. Am. Bull.*, *119*, 917–933, doi:10.1130/B26033.1.

Kidd, W. S. F., Y. S. Pan, C. F. Chang, M. P. Coward, J. F. Dewey, A. Gansser, P. Molnar, R. M. Shackleton, and Y. Y. Sun (1988), Geological mapping of the 1985 Chinese–British (Xizang–Qinghai) Plateau Geotraverse route, *Philos. Trans. R. Soc. London, Ser. A*, *327*, 287–305, doi:10.1098/rsta.1988.0130.

Kohn, M. J., S. K. Pau, and S. L. Corrie (2010), The lower Lesser Himalayan sequence: A Paleoproterozoic arc on the northern margin of the Indian plate, *Geol. Soc. Am. Bull.*, *122*, 323–335, doi:10.1130/B26587.1.

Leech, M. L., S. Singh, A. K. Jain, S. L. Klemperer, and R. M. Manickavasagarn (2005), The onset of India–Asia continental collision: Early, steep subduction required by the timing of UHP metamorphism in the western Himalaya, *Earth Planet. Sci. Lett.*, *234*, 83–97, doi:10.1016/j.epsl.2005.02.038.

Leeder, M. R., A. B. Smith, and J. Yin (1988), Sedimentology, paleoecology, and paleoenvironmental evolution of the 1985 Lhasa to Golmud Geotraverse, *Philos. Trans. R. Soc. London, Ser. A*, *327*, 107–143, doi:10.1098/rsta.1988.0123.

LeFort, P. (1975), Himalayas: The collided range. Present knowledge of the continental arc, *Am. J. Sci.*, *275–A*, 1–44.

LeFort, P. (1996), Evolution of the Himalaya, in *The Tectonic Evolution of Asia*, edited by A. Yin and T. M. Harrison, pp. 95–109, Cambridge Univ. Press, Cambridge, U. K.

LeFort, P., F. Debon, and J. Sonet (1986), The Lower Paleozoic "Lesser Himalayan" granitic belt: Emphasis on the Simchar pluton of central Nepal, in *Granites of the Himalayas, Karakorum, and Hindu Kush*, edited by F. A. Shams, pp. 235–255, Punjab Univ., Lahore, Pakistan.

Leier, A. L., P. Kapp, G. E. Gehrels, and P. G. DeCelles (2007), Detrital zircon geochronology of Carboniferous–Cretaceous strata in the Lhasa terrane, Southern Tibet, *Basin Res.*, *19*, 361–378, doi:10.1111/j.1365-2117.2007.00330.x.

Li, C. (1987), The Longmu Co-Shuanghu-Lancangjiang Suture as the northern boundary of the Gandwanaland in the Carboniferous and Permian, *Bull. Changchun Coll. Geol. Sci.*, *17*, 155–166.

Li, C., and A. Zheng (1993), Paleozoic stratigraphy in the Qiangtang region of Tibet: Relations of the Gondwana and Yangtze continents and ocean closure near the end of the Carboniferous, *Int. Geol. Rev.*, *35*, 797–804, doi:10.1080/00206819309465558.

Li, C., C. Liren, H. Ke, Y. Zengrong, and H. Yurong (1995), *Study on the Paleo-Tethys Suture Zone of Lungmu Co–Shuanghu, Tibet*, 131 pp., Geol. Publ., Beijing.

Li, C., Q. Zhai, Y. Dong, and X. Huang (2006), Discovery of eclogite and its geological significance in Qiangtang area, central Tibet, *Chin. Sci. Bull.*, *51*, 1095–1100, doi:10.1007/s11434-006-1095-3.

Ludwig, K. R. (2008), Isoplot 3.6, *Berkeley Geochronology Cent. Spec. Publ. 4*, 77 pp., Berkeley, Calif.

Marquer, D., H. S. Chawla, and N. Challandes (2000), Pre-Alpine high-grade metamorphism in the High Himalaya crystalline sequences: Evidence from Lower Palaeozoic Kinnaur Kailas granite and surrounding rocks in Sutlej Valley (Himal Ptadesch, India), *Eclogae Geol. Helv.*, *93*, 207–220.

Martin, A. J., P. G. DeCelles, G. E. Gehrels, P. J. Patchett, and C. Isachsen (2005), Isotopic and structural constraints on the location of the Main Central Thrust in the Annapurna Range, central Nepal Himalaya, *Geol. Soc. Am. Bull.*, *117*, 926–944, doi:10.1130/B25646.1.

Martin, A., G. E. Gehrels, and P. G. DeCelles (2007), The tectonic significance of (U, Th)/Pb ages of monazite inclusions in garnet from the Himalaya of central Nepal, *Chem. Geol.*, *244*, 1–24, doi:10.1016/j.chemgeo.2007.05.003.

Martin, A. J., K. D. Burgy, A. J. Kaufman, and G. E. Gehrels (2011), Stratigraphic and tectonic implications of field and isotopic constraints on depositional ages of Proterozoic Lesser Himalayan rocks in central Nepal, *Precambrian Res.*, *185*, 1–17, doi:10.1016/j.precamres.2010.11.003.

Mattinson, C. G., J. L. Wooden, J. G. Liou, D. K. Bird, and C. L. Wu (2006), Age and duration of eclogite-facies metamorphism, North Qaidam HP/UHP terrane, Western China, *Am. J. Sci.*, *306*, 683–711, doi:10.2475/09.2006.01.

McQuarrie, N., D. Robinson, S. Long, T. Tobgay, D. Grujic, G. Gehrels, and M. Ducea (2008), Preliminary stratigraphic and structural architecture of Bhutan: Implications for the along strike architecture of the Himalayan system, *Earth Planet. Sci. Lett.*, *272*, 105–117, doi:10.1016/j.epsl.2008.04.030.

Metcalfe, I. (1988), Origin and assembly of Southeast Asian continental terranes, in *Gondwana and Tethys*, edited by M. G. Audley-Charles and A. Hallam, *Geol. Soc. Spec. Publ.*, *37*, 101–118.

Metcalfe, I. (1996), Gondwanaland dispersion, Asian accretion, and evolution of eastern Tethys, *Aust. J. Earth Sci.*, *43*, 605–623, doi:10.1080/08120099608728282.

Miller, C., M. Tiioni, W. Frank, B. Grasemann, U. Klotzli, P. Guntli, and E. Draganits (2001), The early Palaeozoic magmatic event in the Northwest Himalaya, India: Source, tectonic setting and age of emplacement, *Geol. Mag.*, *138*, 237–251, doi:10.1017/S0016756801005283.

Myrow, P. M., N. C. Hughes, T. S. Paulsen, I. S. Williams, K. R. Thomson, S. A. Bowring, S. C. Peng, and A. D. Ahluwalia (2003), Integrated tectonostratigraphic reconstruction of the Himalaya and implications for its tectonic reconstruction, *Earth Planet. Sci. Lett.*, *212*, 433–441, doi:10.1016/S0012-821X(03)00280-2.

Myrow, P. M., K. R. Thomson, N. C. Hughes, T. S. Paulsen, B. K. Sell, and S. K. Parcha (2006a), Cambrian stratigraphy and depositional history of the northern Indian margin, Spiti Valley, north-central India, *Geol. Soc. Am. Bull.*, *118*, 491–510, doi:10.1130/B25828.1.

Myrow, P. M., K. E. Snell, N. C. Hughes, T. S. Paulsen, N. A. Heim, and S. K. Parcha (2006b), Cambrian depositional history of the Zanskar Valley region of Indian Himalaya: Tectonic Implications, *J. Sediment. Res.*, *76*, 364–381, doi:10.2110/jsr.2006.020.

Myrow, P. M., N. C. Hughes, M. P. Searle, C. M. Fanning, S. C. Peng, and S. K. Parcha (2009), Stratigraphic correlation of Cambrian–Ordovician deposits along the Himalaya: Implications for the age and nature of rocks in the Mount Everest region, *Geol. Soc. Am. Bull.*, *121*, 323–332, doi:10.1130/B26384.1.

Myrow, P. M., N. C. Hughes, J. W. Goodge, C. M. Fanning, I. S. Williams, S. Peng, O. N. Bhargava, S. K. Parcha, and K. R. Pogue (2010), Extraordinary transport and mixing of sediment across Himalayan central Gondwana during the Cambrian–Ordovician, *Geol. Soc. Am. Bull.*, *122*, 1660–1670, doi:10.1130/B30123.1.

Najman, Y., A. Carter, G. Oliver, and E. Garzanti (2005), Provenance of Eocene foreland basin sediments, Nepal: Constraints to the timing and diachroneity of early Himalayan orogenesis, *Geology*, *33*, 309–312, doi:10.1130/G21161.1.

Nie, S., A. Yin, D. Rowley, and Y. Jin (1994), Exhumation of the Dabie Shan ultra-high pressure rocks and accumulation of the Songpan–Ganzi

flysch sequence, *Geology*, 22, 999–1002, doi:10.1130/0091-7613(1994)022<0999:EOTDSU>2.3.CO;2.

Pan, G., L. Ding, D. Yao, and L. Wang (Eds.) (2004), Geologic map of Chinghai–Xizang (Tibet) Plateau and adjacent areas, scale 1:1,500,000, Chengdu Inst. of Geol. and Miner. Res., Geol. Publ., Beijing.

Pan, G. T., X. X. Mo, Z. W. Hou, D. C. Zhu, L. Q. Wang, G. M. Li, Z. D. Zhao, Q. R. Cong, and Z. L. Liao (2006), Spatial–temporal framework of the Gangdese Orogenic Belt and its evolution, *Acta Petrol. Sin.*, 22, 521–533.

Parrish, R. R., and K. V. Hodges (1996), Isotopic constraints on the age and provenance of the Lesser and Greater Himalayan sequences, Nepalese Himalaya, *Geol. Soc. Am. Bull.*, 108, 904–911, doi:10.1130/0016-7606(1996)108<0904:ICOTAA>2.3.CO;2.

Pearce, J. A., and H. Mei (1988), Volcanic rocks of the 1985 Tibet Geotraverse: Lhasa to Golmud, *Philos. Trans. R. Soc., Ser. A*, 327, 169–201.

Pullen, A., P. Kapp, G. Gehrels, J. D. Vervoort, and L. Ding (2008), Triassic continental subduction in central Tibet and Mediterranean-style closure of the Paleo-Tethys Ocean, *Geology*, 36, 351–354, doi:10.1130/G24435A.1.

Pullen, A., P. Kapp, G. Gehrels, L. Ding, and Q.-H. Zhang (2010), Metamorphic rocks in central Tibet: Lateral variations and tectonic implications, *Geol. Soc. Am. Bull.*

Reid, A. J., C. J. L. Wilson, and S. Liu (2005), Structural evidence for the Permo–Triassic tectonic evolution of the Yidun Arc, eastern Tibetan Plateau, *J. Struct. Geol.*, 27(1), 119–137, doi:10.1016/j.jsg.2004.06.011.

Roger, F., J. Malavieile, P. H. Leloup, S. Calassou, and Z. Xu (2004), Timing of granite emplacement and cooling, in the Songpan–Garze fold belt (eastern Tibet Plateau) with tectonic implications, *J. Asian Earth Sci.*, 22, 465–481, doi:10.1016/S1367-9120(03)00089-0.

Sakai, H. (1991), The Gonwanas in the Nepal Himalaya, in *Sedimentary Basins of India: Tectonic Context*, edited by S. K. Tandon, C. C. Pant, and S. M. Casshyap, pp. 202–217, Gyanodaya Prakashan, Nainital, India.

Searle, M. P., B. F. Windley, M. P. Coward, D. J. W. Cooper, A. J. Rex, T. Li, X. Xiao, M. Q. Jan, V. C. Thakur, and S. Kumar (1987), The closing of the Tethys and the tectonics of the Himalaya, *Geol. Soc. Am. Bull.*, 98, 678–701, doi:10.1130/0016-7606(1987)98<678:TCOTAT>2.0.CO;2.

Şengör, A. M. C. (1979), Mid-Mesozoic closure of Permo–Triassic Tethys and its implications, *Nature*, 279, 590–593, doi:10.1038/279590a0.

Şengör, A. M. C., and B. A. Natal'in (1996a), Paleotectonics of Asia: Fragments of a synthesis, in *The Tectonic Evolution of Asia*, edited by A. Yin and T. M. Harrison, pp. 486–640, Cambridge Univ. Press, New York.

Şengör, A. M. C., and B. A. Natal'in (1996b), Turkic-type orogeny and its role in making of the continental crust, *Annu. Rev. Earth Planet. Sci.*, 24, 263–337, doi:10.1146/annurev.earth.24.1.263.

Şengör, A. M. C., D. Altiner, A. Cin, T. Ustaomer, and K. J. Hsü (1988), Origin and assembly of the Tethyside orogenic collage at the expense of Gondwana Land, in *Gondwana and Tethys*, *Geol. Soc. Spec. Publ.*, 37, 119–181.

She, Z., C. Ma, R. Mason, J. Li, G. Wang, and Y. Lei (2006), Provenance of the Triassic Songpan–Ganzi flysch, west China, *Chem. Geol.*, 231(1–2), 159–175, doi:10.1016/j.chemgeo.2006.01.001.

Sobel, E. R., and N. Arnaud (1999), A possible middle Paleozoic suture in the Altyn Tagh, NW China, *Tectonics*, 18(1), 64–74, doi:10.1029/1998TC900023.

Stacey, J. S., and J. D. Kramers (1975), Approximation of terrestrial lead isotope evolution by a two stage model, *Earth Planet. Sci. Lett.*, 26, 207–221, doi:10.1016/0012-821X(75)90088-6.

Stampfli, G. M., and G. D. Borel (2002), A plate tectonic model for the Paleozoic and Mesozoic constrained by dynamic plate boundaries and restored synthetic oceanic isochrones, *Earth Planet. Sci. Lett.*, 196, 17–33, doi:10.1016/S0012-821X(01)00588-X.

Stern, R. J. (1994), Arc-Assembly and Continental Collision in the Neoproterozoic African Orogen: Implications for the Consolidation of Gondwanaland, *Annu. Rev. Earth Planet. Sci.*, 22, 319–351, doi:10.1146/annurev.ea.22.050194.001535.

Stöcklin, J. (1980), Geology of Nepal and its regional frame, *J. Geol. Soc.*, 137, 1–34.

Stöcklin, J., and K. D. Bhattarai (1977), Geology of the Kathmandu area and central Mahabharat Range, Nepal, Himalaya, technical report, 86 pp., Nepal Dep. of Mines and Geol., Kathmandu.

Torsvik, T. H., and L. R. M. Cocks (2009), The Lower Palaeozoic palaeogeographical evolution of the northeastern and eastern peri-Gondwanan margin from Turkey to New Zealand, in *Early Paleozoic Peri-Gondwana Terranes: New Insights From Tectonics and Biogeography*, edited by M. G. Bassett, *Geol. Soc. Spec. Publ.*, 325, 3–21.

Upreti, B. N. (1999), An overview of the stratigraphy and tectonics of the Nepal Himalaya, *J. Asian Earth Sci.*, 17, 577–606, doi:10.1016/S1367-9120(99)00047-4.

Wang, G.-C., R. P. Wintsch, J. I. Garver, M. Roden-Tice, S.-F. Chen, K.-X. Zhang, Q.-X. Lin, Y.-H. Zhu, S.-Y. Xiang, and D.-W. Li (2009), Provenance and thermal history of the Bayan Har Group in the western-central Songpan–Ganzi–Bayan Har terrane: Implications for tectonic evolution of the northern Tibetan Plateau, *Isl. Arc*, 18, 444–466, doi:10.1111/j.1440-1738.2009.00666.x.

Webb, A., A. Yin, T. M. Harrison, J. Célérier, and P. Burgess (2007), The leading edge of the Greater Himalayan Crystalline complex revealed in the NW Indian Himalaya: Implications for the evolution of the Himalayan orogen, *Geology*, 35(10), 955–958, doi:10.1130/G23931A.1.

Weislogel, A. L. (2008), Tectonostratigraphic and geochronologic constraints on evolution of the northeast Paleotethys from the Songpan–Ganzi complex, central China, *Tectonophysics*, 451, 331–345, doi:10.1016/j.tecto.2007.11.053.

Weislogel, A. L., S. A. Graham, E. Z. Chang, J. L. Wooden, G. E. Gehrels, and H. Yang (2006), Detrital zircon provenance of the Late Triassc Songpan–Ganzi complex: Sedimentary record of collision of the North and South China blocks, *Geology*, 34, 97–100, doi:10.1130/G21929.1.

Weislogel, A. L., S. A. Graham, E. Z. Chang, J. L. Wooden, and G. E. Gehrels (2010), Detrital zircon provenance from three turbidite depocenters of the Middle–Upper Triassic Songpan–Ganzi complex, central mChina: Record of collision tectonics, erosional exhumation, and sediment production, *Geol. Soc. Am. Bull.*, 122, 1969–1990.

Xiao, W. J., B. F. Windley, H. L. Chen, G. C. Zhang, and J. L. Li (2002), Carboniferous–Triassic subduction and accretion in the western Kunlun, China: Implications for the collisional and accretionary tectonics of the northern Tibetan Plateau, *Geology*, 30(4), 295–298, doi:10.1130/0091-7613(2002)030<0295:CTSAAI>2.0.CO;2.

Xu, R. H., U. Schärer, and C. J. Allégre (1985), Magmatism and metamorphism in the Lhasa block (Tibet): A geochronological study, *J. Geol.*, 93, 41–57, doi:10.1086/628918.

Yang, J., Z. Xu, Z. Li, X. Xu, T. Li, Y. Ren, H. Li, S. Chen, and P. T. Robinson (2009), Discovery of an eclogite belt in the Lhasa block, Tibet: A new border for Paleo-Tethys?, *J. Asian Earth Sci.*, 34, 76–89, doi:10.1016/j.jseaes.2008.04.001.

Yin, A. (2006), Cenozoic tectonic evolution of the Himalayan orogen as constrained by along-strike variation of structural geometry, exhumation history, and foreland sedimentation, *Earth Sci. Rev.*, 76, 1–131, doi:10.1016/j.earscirev.2005.05.004.

Yin, A., and T. M. Harrison (2000), Geologic evolution of the Himalayan–Tibetan orogen, *Annu. Rev. Earth Planet. Sci.*, 28, 211–280, doi:10.1146/annurev.earth.28.1.211.

Yin, A., and S. Nie (1993), An indentation model for North and South China collision and the development of the Tanlu and Honan fault systems, eastern Asia, *Tectonics*, 12, 801–813, doi:10.1029/93TC00313.

Yin, A., and S. Nie (1996), A Phanerozoic palinspastic reconstruction of China and its neighboring regions, in *The Tectonics of Asia*, edited by A. Yin and T. M. Harrison, pp. 442–485, Cambridge Univ. Press, New York.

Yin, A., C. E. Manning, O. Lovera, C. Menold, X. Chen, and G. E. Gehrels (2007), Early Paleozoic tectonic and thermomechanical evolution of ultrahigh-pressure (UHP) metamorphic rocks in the northern Tibetan Plateau, northwest China, *Int. Geol. Rev.*, 49, 681–716, doi:10.2747/0020-6814.49.8.681.

Yin, A., C. S. Dubey, T. K. Kelty, A. A. G. Webb, T. M. Harrison, C. Y. Chou, and J. Célérier (2010a), Geologic correlation of the Himalayan orogen and Indian craton: Part 2. Structural geology, geochronology, and tectonic evolution of the Eastern Himalaya, *Geol. Soc. Am. Bull.*, 122, 360–395, doi:10.1130/B26461.1.

Yin, A., C. S. Dubey, A. A. G. Webb, T. K. Kelty, M. Grove, G. E. Gehrels, and W. P. Burgess (2010b), Geologic correlation of the Himalayan orogen and Indian craton: Part 1. Structural geology, U-Pb zircon geochronology, and tectonic evolution of the Shillong Plateau and its neighboring regions in NE India, *Geol. Soc. Am. Bull.*, 122, 336–359, doi:10.1130/B26460.1.

Yoshida, M., and B. Upreti (2006), Neoproterozoic India within east Gondwana: Constraints from recent geochronologic data from Himalaya, *Gondwana Res.*, 10, 349–356, doi:10.1016/j.gr.2006.04.011.

Zhang, K.-J. (2001), Blueschist-bearing metamorphic core complexes in the Qiangtang block reveal deep crustal structure of northern Tibet: Comment, *Geology*, 29, 90, doi:10.1130/0091-7613(2001)029<0090:BBMCCI>2.0.CO;2.

Zhang, K.-J., and X. Tang (2009), Eclogites in the interior of the Tibetan Plateau and their geodynamic implications, *Chin. Sci. Bull.*, 54, 2556–2567, doi:10.1007/s11434-009-0407-9.

Zhang, K.-J., J.-W. Cai, Y.-X. Zhang, and T.-P. Zhao (2006a), Eclogites from central Qiangtang, northern Tibet (China) and tectonic implications, *Earth Planet. Sci. Lett.*, 245, 722–729, doi:10.1016/j.epsl.2006.02.025.

Zhang, K.-J, Y.-X. Zhang, B.-D. Xia, and Y.-B. He (2006b), Temporal variations of Mesozoic sandstone compositions in the Qiangtang block,

northern Tibet (China): Implications for provenance and tectonic setting, *J. Sediment. Res.*, *76*(8), 1035–1048, doi:10.2110/jsr.2006.089.

Zhou, D., and S. A. Graham (1996), The Songpan–Ganzi complex of the west Qinling Shan as a Triassic remnant ocean basin, in *The Tectonics of Asia*, edited by A. Yin and T. N. Harrison, pp. 281–299, Cambridge Univ. Press, New York.

Zhu, D.-C., X.-X. Mo, Y. Niu, Z.-D. Zhao, L.-Q. Wang, G.-T. Pan, and F.-Y. Wu (2009), Zircon U-Pb dating and in-situ Hf isotopic analysis of Permian peraluminous granite in the Lhasa terrane, southern Tibet: Implications for Permian collisional orogeny and paleogeography, *Tectonophysics*, *469*, 48–60, doi:10.1016/j.tecto.2009.01.017.

Zhu, D.-C., X.-X. Mo, Z.-D. Zhao, Y. Niu, L.-Q. Wang, Q.-H. Chu, G.-T. Pan, J.-F. Xu, and C.-Y. Zhou (2010), Presence of Permian extension- and arc-type magmatism in southern Tibet: Paleogeographic implications, *Geol. Soc. Am. Bull.*, *122*, 979–993, doi:10.1130/B30062.1.

_____

R. Blakey, Department of Geology, Northern Arizona University, Flagstaff, AZ 86011, USA. (ronald.blakey@nau.edu)

P. DeCelles, G. Gehrels, P. Kapp, and A. Pullen, Department of Geosciences, University of Arizona, Gould-Simpson Bldg. 77, 1040 E. 4th St., Tucson, AZ 85721, USA. (decelles@email.arizona.edu; ggehrels@email.arizona.edu; pkapp@email.arizona.edu; apullen@email.arizona.edu)

L. Ding, Institute of Tibetan Plateau Research, Chinese Academy of Sciences, Beijing 100029, China. (dinglin@itpcas.ac.cn)

J. Guynn, ExxonMobil Exploration Company, Houston, TX 77060, USA. (jeromeguynn@gmail.com)

A. Martin, Department of Geology, University of Maryland, College Park, MD 20742, USA. (martinaj@geol.umd.edu)

N. McQuarrie, Department of Geological Sciences, Princeton University, Guyot Hall, Princeton, NJ 08544, USA. (nmcq@princeton.edu)

A. Weislogel, Department of Geological Sciences, University of Alabama, Tuscaloosa, AL 35487, USA. (aweislogel@geo.ua.edu)

A. Yin, Department of Earth and Space Sciences, University of California, 595 Charles Young Dr., Geology Bldg., Rm. 4676, Los Angeles, CA 90095-1567, USA. (yin@ess.ucla.edu)